MATERIALS CHEMISTRY FRONTIERS

REVIEW

View Article Online
View Journal





Cite this: DOI: 10.1039/d1qm00035g

# Transition metal dichalcogenide-decorated MXenes: promising hybrid electrodes for energy storage and conversion applications

N. R. Hemanth, †[a] Taekyung Kim, †[b] Byeongyoon Kim, †[b] Arvind H. Jadhav, [c] Kwangyeol Lee *[b] and Nitin K. Chaudhari *[d]

Received 8th January 2021,
Accepted 16th February 2021

DOI: 10.1039/d1qm00035g

rsc.li/frontiers-materials

Various two-dimensional (2D) materials have demonstrated unique structure-dependent characteristics that are conducive to energy-harvesting applications. Among them, the family of layered MXenes has found a wide range of applications in batteries, supercapacitors, photo- and electrocatalysis, water purification, biosensors, electromagnetic interference shielding, structural composites, *etc.*, owing to their well-defined structure, large surface area, large interlayer distance, and excellent thermal and electrical conductivity. However, layer restacking due to hydrogen bonding or van der Waals forces between the layers considerably impedes the utility of MXenes. To tackle the restacking issues, transition metal dichalcogenides (TMDs) such as $MoS_2$, $WS_2$, and $MoSe_2$ nanosheets have been uniformly dispersed on the surface of MXenes, which not only mitigates the restacking of the MXenes but also improves the electrochemical performance due to the synergistic interaction between MXenes and TMDs. This review describes recent advances in the synthesis of MXene/TMD heterostructures and the nature of the synergistic interactions between TMDs and MXenes in energy-related applications. We further highlight future research directions for MXene/TMD-based materials for energy storage applications.

[a] *Department of Metallurgical and Materials Engineering, National Institute of Technology Karnataka (NITK), Surathkal, Karnataka 575025, India*
[b] *Department of Chemistry and Research Institute for Natural Sciences, Korea University, Seoul, 02841, Republic of Korea. E-mail: kylee1@korea.ac.kr*
[c] *Centre for Nano and Material Science (CNMS), Jain University, Jain Global Campus, Bangalore 562112, Karnataka, India*
[d] *Department of Chemistry, School of Technology, Pandit Deendayal Petroleum University, Gandhinagar 382007, Gujarat, India. E-mail: nitin.chaudhari@sot.pdpu.ac.in*
† These authors contributed equally to this work.

**N. R. Hemanth**

*N. R. Hemanth is a final year undergraduate student pursuing a bachelor's degree in metallurgical and materials engineering, at National Institute of Technology Karnataka, Surathkal, India. His research interests include 2D-based nanomaterials, functional polymeric materials and composites for specialized industrial applications. His other research interests include nanomaterials for energy harvesting applications.*

**Taekyung Kim**

*Dr Taekyung Kim earned his PhD degree (2020) in inorganic chemistry from Korea University after working at Kolon Industries, Inc., (Republic of Korea) as an engineer for several years. Currently, his research interests are mainly focused on the development of synthetic methods for phase and structure-controlled nanocatalysts and their potential applications in electrocatalytic water splitting.*

# 1. Introduction

Energy and environmental issues have reached crisis levels over the last decade due to the rapid depletion of fossil fuels and the associated climate changes.[1] To address these challenges, it is imperative to develop sustainable energy production technologies by tapping into renewable energy sources such as solar, geothermal, and wind energy. The development of electrochemical storage devices such as batteries, supercapacitors, and water electrolyzers for converting hydrogen to electrical energy, as well as fuel cells for efficient conversion of chemical energy in hydrogen to electricity, is critical.[2]

In recent years, atomically thin two-dimensional (2D) materials have attracted considerable interest owing to their unmatched portfolio of optical, electrical, and mechanical properties.[3] Among the plethora of 2D materials, transition metal carbides/nitrides (MXenes), the newest additions to the family of 2D materials, have been prepared by the selective extraction of element 'A' from layered hexagonal MAX precursors using hydrogen fluoride as an etching agent, or from layered ceramics.[4] The large surface area, tunable interlayer distance, and narrow diffusion barrier, combined with the superior metallic conductivity of MXenes, make them optimal electrode materials.[5] However, MXene layers undergo restacking, which limits their potential utility in electrochemical applications.[6] Therefore, for further enhancement of the electrochemical performance, spacers have been introduced between the layers of MXenes to develop a porous structure. The introduction of nano-carbon, conductive polymers, heteroatoms, metal oxides, and TMDs considerably increased the interlayer distance to yield better electrochemical performance.[7] On the other hand, transition metal dichalcogenides (TMDs) have been extensively explored as electrode materials in the past decade due to their large specific area, excellent electrical properties, atomically thin layered arrangement,

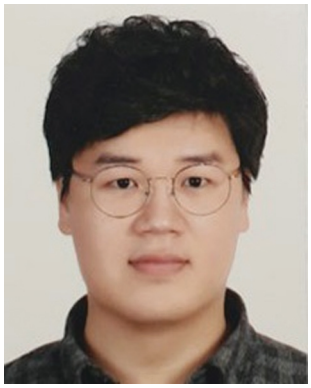

**Byeongyoon Kim**

*Dr Byeongyoon Kim received his PhD Degree (2018) in inorganic chemistry from Korea University, Republic of Korea. Currently, he is working as a postdoctoral fellow with Prof. Kwangyeol Lee at Nano Chemistry Laboratory, Korea University. His research interests include the design and synthetic methodology for transition metal-based functional nanomaterials and the applications of electrocatalysis.*

**Arvind H. Jadhav**

*Dr Arvind H. Jadhav is currently working as an Assistant Professor at the Centre for Nano and Material Sciences (CNMS), JAIN University, India. He received his PhD from Myongji University, Republic of Korea. Dr Jadhav has several research publications to his credit in reputed peer reviewed international journals. He is also a recipient of many awards for his academic excellence with a gold medal for his PhD research and a good number of best paper and best poster presentation awards. His research areas focus on heterogeneous catalysis for $CO_2$ conversion and utilisation, synthesis of ILs for organic transformations, and sustainable energy applications.*

**Kwangyeol Lee**

*Professor Kwangyeol Lee obtained his PhD degree (1997) in chemistry from the University of Illinois at Urbana- Champaign. After fulfilling his military obligation, he joined Korea University in 2003 as a chemistry faculty member, before being appointed as a professor. He is the recipient of the 2009 Wiley-KCS Young Scholar Award. His current interests include the development of synthetic methodologies for nanoscale materials, the application of nanomaterials in biomedical fields, and the development of nanotechnologies to support the environment by creating sustainable energy sources.*

**Nitin K. Chaudhari**

*Dr Nitin Chaudhari is an Associate Professor at Pandit Deendayal Petroleum University, Gandhinagar, India. He received his PhD degree in materials science from Korea University, South Korea in 2013. He subsequently worked as a research professor at Myongji University and Korea University, South Korea from 2013 to 2019. Later, he joined Nexcoms Ltd. Co., South Korea as Deputy Director before moving to India. His research interest includes the design and development of active electrode materials such as porous carbons, nanocomposites, oxides, sulphides, hydroxides, 2D MXenes, and nanomaterials for energy storage and conversion devices.*

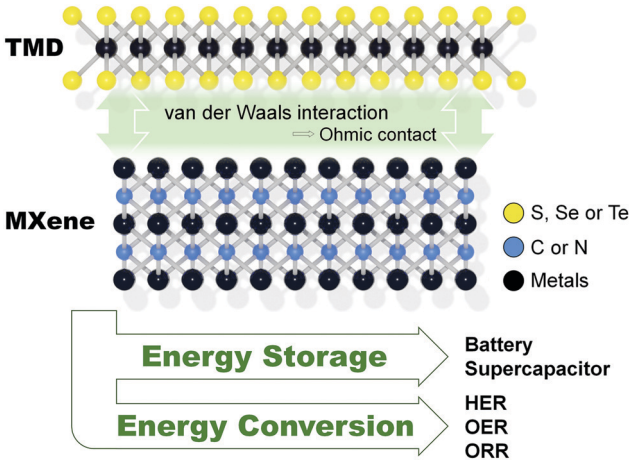


Fig. 1 A graphical abstract of the 2D TMD/MXene hybrid structure toward energy storage and conversion.

and stability.[8] However, TMDs suffer from poor cycling stability, low electrical conductivity, and, most critically, a limited number of active sites located on the edges, which seriously limits the catalytic performance of TMDs.[9] Recent studies show that combining the 2D structures of MXenes and TMDs can preserve the best features of both the MXenes and TMDs. When MXenes are combined with TMDs, restacking of the layers is hindered, thereby increasing the contact area between the electrolyte and electrode.[7a,10] Moreover, the 2D heterointerface between MXenes and TMDs consists of van der Waals interactions that can prevent Fermi level pinning; this effect operates synergistically with the work function adjustability of metallic MXenes to afford Schottky barrier-free contact and reduce the contact resistance.[11] The MXene–TMD composites demonstrated excellent reversible specific capacitance, superior coulombic efficiency, and improved cyclability and rate performance in electrochemical applications (Fig. 1).

An extensive literature survey reveals the existence of several review papers on the respective topics concerning MXenes and TMDs.[4c,8,12] However, no critical review article on MXene/TMD composites is available, although this unique heterostructure family has great potential as electrochemical materials; thus, a timely account of this topic would be greatly helpful to researchers in related fields. The present review highlights the recent developments in the fabrication and electrochemical applications of MXene/TMD composites. Furthermore, the electronic structure and ion transfer mechanism are explained using density functional theory (DFT). Finally, we summarize the present research on MXene composites to provide overall prospects for this material family and trigger rapid development in this exciting material class for future energy applications.

## 2. MXenes and TMDs

### 2.1 Transition metal carbides/nitrides (MXenes)

**2.1.1 Synthesis.** Two-dimensional transition metal carbides or nitrides, referred to as MXenes, are an emerging family of metallic or semiconducting materials possessing electrical conductivity and a hydrophilic surface.[13] They are usually represented by the formula $M_{n+1}X_nT_x$ ($n$ = 1, 2 or 3), where M refers to an early transition metal (M = Sc, Ti, V, Cr, Zr, Nb, Mo, Hf, and Ta), X denotes carbon or nitrogen, and T stands for surface terminal groups (T = $OH^-$, $F^-$, and $O^{2-}$).[14] MXenes are synthesized by the selective removal of the A-group (mostly elements of IIIA and IVA groups of the periodic table) from layered hexagonal ternary carbides known as MAX phases (Fig. 2).[15] MAX powders are immersed in a controlled quantity of hydrofluoric acid (HF) solution at room temperature or higher temperature, resulting in the formation of surface terminals on MXenes, which are mainly oxygen and/or hydroxyl moieties.[16] Since the direct handling of HF is dangerous due to its toxic nature, a safer *in situ* formation of HF has been accomplished through the reaction of HCl and fluoride salts or *via* ammonium bifluoride. These HF precursors aid in the simultaneous intercalation of cations like $Li^+$, $Na^+$, $K^+$, $NH_4^+$, $Ca^+$, and $Al^{3+}$ between the interlayers.[15,17] The intercalation of the cation and water during this process results in delamination without any additional steps, which is another advantage of *in situ* HF over the pure HF etching method. The etching conditions for the complete transition of MAX to MXene depend on different variables; the M–Al bond strength in Al-based MAX phases determines the etching environment, and the increasing number $n$ in $M_{n+1}C_nT_x$ type requires stronger and/or longer etching conditions. On the other hand, nitride-based MXenes have been prepared using molten fluoride salts for etching the A-elements from MAX precursors at a relatively higher temperature (at 550 °C) under argon atmosphere.[4c,18] Synthesis of MXenes by chemical vapor deposition (CVD) is also possible, where high-quality ultra-thin orthorhombic α-$Mo_2C$ crystals with a lateral size of ~100 μm were produced from the decomposition of methane on a bilayer substrate comprising copper foil placed over molybdenum foil. This method was further applied to the fabrication of WC and TaC crystals.[19] Until now, various bottom-up synthesis methods such as CVD, template methods, plasma-enhanced pulsed laser deposition, *etc.*, have been reported to produce higher quality crystals compared to selective etching processes.[20] While ultra-thin MXenes have been obtained by bottom-up synthesis, single-layered MXenes have not yet been demonstrated by these processes. MXenes can also be prepared from non-MAX phase precursors by etching the Al–C units from $M_nAl_3C_2$ and $M_nAl_4C_{n+3}$.[21] Furthermore, it has been reported that etching of Al–C units together is energetically more favorable than etching of single Al units. Delamination of MXenes is a crucial step to the understanding of their fundamental properties, and is also necessary for the fabrication of MXene-based electrodes with high storage capacity.[21a] Before delamination, the structure of multilayered MXenes is similar to that of graphene-like stacks of sheets, and delamination of multilayered MXenes into few-layered or mono-layered nanosheets using an organic base drastically improves the accessibility to the surface.[22] Due to strong interlayer forces, delamination of multilayered MXenes by mechanical exfoliation is more difficult than those of graphite and $MoS_2$, and results in poor yield of mono-layers of MXenes.[23] Therefore, delaminating by intercalation of various organic,

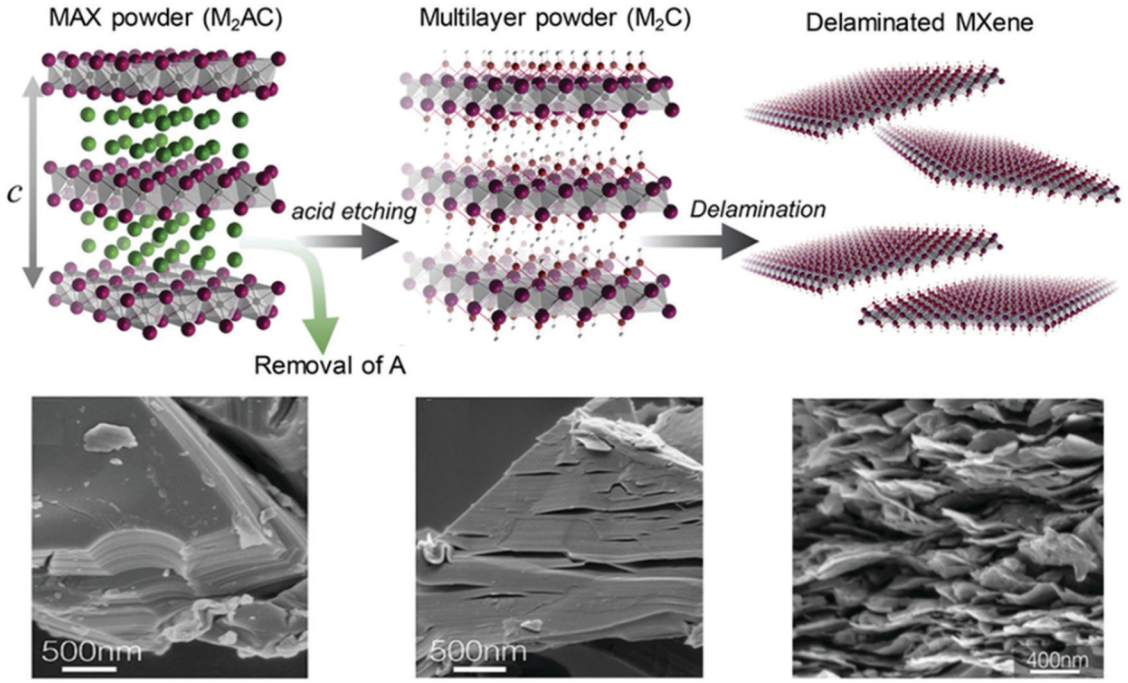


Fig. 2 Typical synthesis of MXene from MAX phase *via* the selective etching method and its delaminated structure; the bottom SEM images represent MAX, MXene and delaminated-MXene structures, respectively. Reproduced with permission.[113] Copyright 2020, Wiley.

inorganic, and ionic species followed by sonication has been widely practiced, because of large-scale production of single MXene layers.[16,22a,22b]

**2.1.2 Structure and properties.** The MXene crystal structure is similar to that of the parent MAX phases; the mono-layer of MXene comprises a hexagonal lattice with six-fold symmetry, wherein the transition metal ions are six-coordinate.[24] The remarkable properties of MXenes include excellent thermal and electrical conductivity, a high Young's modulus, and a tunable bandgap.[25] The surface termination is an important factor in determining the mechanical properties of MXenes. For example, a recent study has revealed that the O-terminated MXenes display better mechanical strength, mainly due to the stronger bonding between M–O than M–F and M–OH.[26] Thin MXene films are transparent and conduct electricity, and this unique combination of properties makes them novel materials for transparent conductive electrodes as well.[27] However, the synthesis process and composition can affect the electronic conductivity of MXene; larger flakes with minimum defects have displayed higher conductivity. Furthermore, high-quality single flakes and O/OH-terminated MXenes are more stable towards oxidation. Pristine MXenes display metallic character, but their metallic nature decreases as the number of layers increases. In addition, a few MXene materials become semiconducting after surface modification.[28] MXenes are unique among two-dimensional materials, including graphene, because of their notable hydrophilic surface and exceptional metallic conductivity.[29] Density functional theory predicts that the pristine MXene would exhibit magnetic behavior due to the presence of Ti atoms on the surface. With the surface termination step, the MXene loses its magnetic property.[30]

The appealing properties of MXenes lead to a wide range of applications, including chemical adsorption, electromagnetic interference (EMI) shielding, biomedical applications, wastewater treatment, and environmental remediation.[13,31] MXenes have shown great potential as electro/photocatalysts for hydrogen evolution reactions, and $CO_2$ reduction reactions, and as electrode materials for supercapacitors and batteries.[32] However, the low capacitance of the resulting anodes, complex surface functionalities, and oxidation of MXenes limit their applications.[4b,7a,33]

## 2.2 Transition metal dichalcogenides (TMDs)

**2.2.1 Synthesis.** Two-dimensional transition metal dichalcogenides are intriguing semiconducting layered materials with the typical formula $MX_2$, where M denotes a transition metal atom of group VI of the periodic table (*e.g.*, Mo or W), whereas X is a chalcogen atom (S, Se, or Te).[8b] Mechanical exfoliation, in which a layer is peeled off from the bulk crystals using adhesive Scotch tape, is a clean and rapid method for producing high-quality crystalline and atomically thin mono-layers of TMDs. However, this method produces a non-uniform flake size, the deposited material is non-uniform, and it is difficult to separate the layers.[34] To overcome these problems, nanolayers of bulk TMD crystals are produced by liquid-phase exfoliation by ultrasonication in organic solvents, in which the nanolayers remain chemically unaltered, and their electronic properties are maintained.[35] Recently, aqueous ammonia has been used as an alternative and eco-friendly solvent for scalable liquid-phase exfoliation of $MoS_2$ and $WS_2$.[36] Furthermore, this solvent offers high concentration yields with good stoichiometry, structural

 

and semiconductor qualities, and does not require additional surfactants and stabilizers. High-quality ultra-thin TMDs can also be prepared from a molecular beam epitaxy (MBE) method in an ultrahigh vacuum chamber with high purity source materials (Fig. 3a).[37] The low growth temperature, low deposition rate, and *in situ* characterization during the MBE process provide good synthetic control with minimal impurities in the final TMD films. Bottom-up synthesis routes are the most practical approaches to 2D TMDs because they afford a high yield, precise control over the lateral size, and a homogeneous composition and structure of the nanolayers.[8b] Chemical vapor deposition is widely considered as a scalable method of developing thin 2D TMDs and their heterostructures (Fig. 3b), due to the great control over the morphology and low cost. As a result, several $MX_2$ type TMDs with excellent semiconducting properties have been synthesized. The earliest and primary method reported employs the vapor-phase reaction of the parent metal oxide ($WO_3$, or $MoO_3$) and chalcogen element at high temperature by co-evaporation, leading to the growth of thin stable TMDs on the substrate.[38] In addition to various growth parameters of CVD such as temperature, growth time, and atomic gas flux, growth substrate and system design are also important for controlled and optimized growth of 2D TMDs.[39] Furthermore, by increasing the density of edge sites during the mid-growth process and by creating vacancies to activate the basal plane in the post-growth process, the catalytic activity of CVD-grown TMDs can be enhanced.[40] Another CVD growth occurs *via* a two-step process, where the pre-deposited metal precursor on the substrate reacts with a gaseous vapor of sulfur, selenium, or tellurium in an inert atmosphere.[41] Synthesis of large-area, thin, crystalline TMDs on various insulating substrates has been accomplished by the thermolysis process, in which the crystallinity increases sharply upon the addition of sulfur during high-temperature annealing of thermally decomposed salts.[42] Better control might be achieved by metal–organic chemical vapor deposition (MOCVD), in which metal–organic or organosulfur precursors are used to develop wafer-scale films with high crystallinity (Fig. 3c). Precise control over the gas-phase precursors helps in tuning the domain size, shape, and nucleation density. However, the noxious precursors and slow deposition are the main drawbacks of this process.[43] Recently a novel growth-etch MOCVD process has been presented to eliminate the carbon contamination and small domain size resulting from the conventional MOCVD process, wherein introducing water vapor during the process has improved the final crystal quality.[44] Atomic layer deposition by a gas-phase reaction of the parent elements has recently been used to prepare conformal, thin, binary transition metal sulfides on various substrates, including 3D templates.[45] The uniform, area selective growth of 2D thin TMD films has been achieved by controlling the incubation period on various substrates or by using the ABC-type plasma-enhanced ALD process.[46]

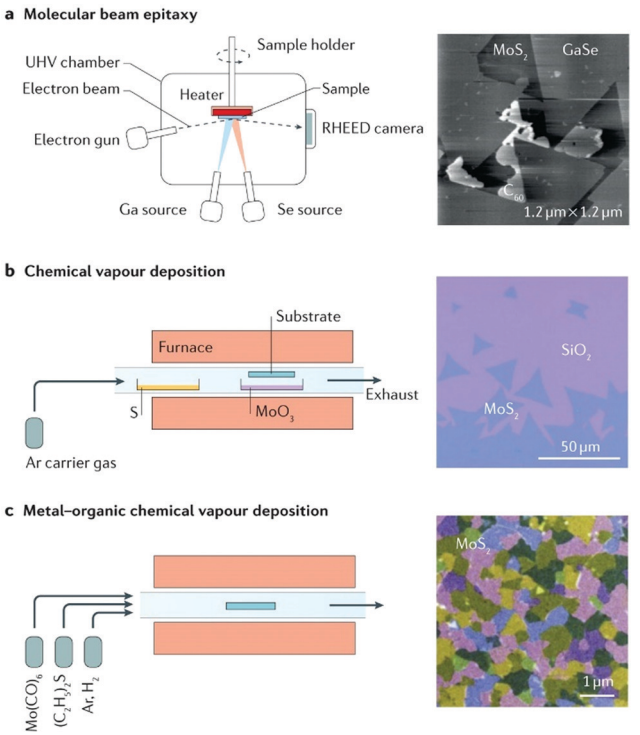


Fig. 3 (a) Schematic illustration of a molecular beam epitaxy process with atomic force microscopy image of GaSe mono-layer grown on $MoS_2$. (b) Schematic illustration of chemical vapour deposition with an optical image of $MoS_2$ domains grown on $SiO_2$. (c) Schematic illustration of metal–organic chemical vapour deposition with a false-colour dark field transmission electron microscopy image of the $MoS_2$ mono-layer having different grain orientation. (a), (b) and (c) Reproduced with permission.[8b] Copyright 2017, Macmillan Publishers Limited.

**2.2.2 Structure and properties.** The crystal structure of single-layer TMDs ($MX_2$) comprises a transition metal layer (M) sandwiched between two atomic layers of chalcogen (X).[47] A triangular prismatic phase (2H) and an octahedral phase (1T) are the two commonly observed phases. The thermodynamically stable 2H-$MoS_2$ exhibits six-siemens atoms prismatically surrounding each of the Mo atoms, and the metastable 1T-$MoS_2$ comprises six-siemens atoms surrounding each of the Mo atoms in the form of a distorted octahedron.[48] Each of these phases exhibits distinctively different electronic properties, as 2H-$MoS_2$ is semiconducting, whereas 1T-$MoS_2$ is a metallic and more active hydrogen evolution catalyst.

The Young's modulus of defect-free single-layer $MoS_2$ is comparable to that of stainless steel, and therefore monolayer $MoS_2$ can be used as a reinforcing component in composite materials.[49] The unique functionalities of 2D TMDs allow them to transform the indirect bandgap in multilayered TMDs to a direct bandgap in single-layered TMDs with good carrier mobility.[50] The unique properties of TMDs have led to many phenomenal applications. The tunable bandwidth of monolayer TMDs has been extensively utilized in the field of high-performance flexible electronics and optoelectronics.[51] The inactive basal plane in $MoS_2$ (typical TMD) impedes the trapping of $Li^+$ on the surface, and thus the coulombic efficiency of $MoS_2$ anodes is far superior to that of graphene oxide and its derivatives.[9a] The desirable characteristics of high capacitance and stability have also been observed in other TMDs, which has led to widespread interest and advances in the domain of energy storage and conversion.[52] The morphologies of 2D TMDs, thermal stability, conductivity, mechanical features, tunable bandgap, and their direct influence

on the optical properties of materials have inspired a broad range of applications in sensors,[53] catalysis for hydrogen evolution,[54] flexible electronics and optoelectronics,[51,55] and energy storage.[56] However, developing routes for the synthesis of structures with more active sites in the basal plane remains a significant challenge. Furthermore, the electrochemical stability and electrical conductivity are far from satisfactory.

On the other hand, coupling TMDs with MXenes reportedly allows the full exploitation of the extraordinary features of each component. The TMD/MXene heterostructure demonstrated outstanding specific capacitance, durable performance, enhanced coulombic efficiency, satisfactory reverse capacitance at high current rates, and enhanced ion transport and structural stability during redox reactions.[57]

## 3. Synergy between MXene and TMDs

When combining two different materials to obtain a heterostructure, synergetic interaction between the different material phases is generally expected. Although the effort to combine TMDs and MXenes is in the very early stage, synergistic interaction between these materials has been demonstrated in a number of examples.[58] When a junction is formed by a metal and semiconductor contact, it creates a potential barrier for charge carriers to cross the junction, the so-called Schottky barrier (SB), which ideally follows the predictions of the Schottky–Mott model:

$$\Phi_{B,n} = \phi_M - \chi_S, \Phi_{B,p} = I_S - \phi_M (\text{Schottky} - \text{Mott}) \quad (1)$$

where $\Phi_{B,n}$ and $\Phi_{B,p}$ are the n-type and p-type SB height (SBH), and $\chi_s$ and $I_s$ are the electron affinity and ionization energy of the semiconductor, respectively.[59] The SBH should be as low as possible to reduce the contact resistance of the metal–semiconductor junction (MSJ), and ultimately be zero or negative to achieve SB-free contact. Because most electrode metals do not meet the above criteria, investigations of electrode materials with tunable work functions have recently been emphasized for 2D TMD semiconductor devices. The work function of MXenes varies over a wide range with the surface functional groups, composition, and thickness. Based on first-principles calculations, Liu *et al.* reported that the work function of MXenes with OH- and O-terminations on their surface is smaller than that of Sc (3.5 eV) and larger than that of Pt (5.6 eV), respectively, (Fig. 4).[60] Mixing of O and OH or adding F terminations brings the work function to a moderate level, allowing the use of the material as a work function regulator.

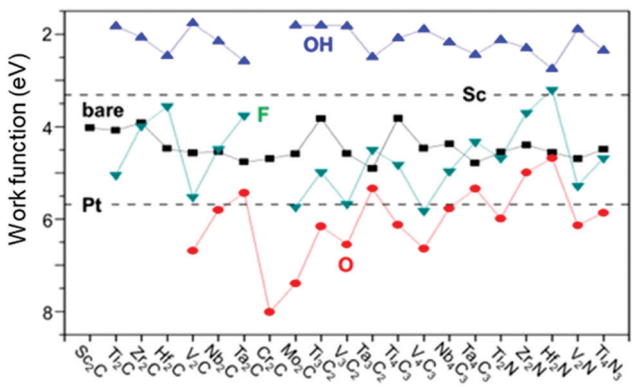


Fig. 4 Work function plots of MXenes with OH-, F- and O- terminations. Reproduced with permission.[60] Copyright 2016, American Chemical Society.

Although the work function of electrode metals seems to be a suitable descriptor of the SBH in MSJ, studies have revealed that the measured SBH is not directly proportional to the metal work function, which deviates from the Schottky–Mott rule.[61] This discrepancy is attributed to Fermi level pinning (FLP), driven by various gap states, including surface states, metal-induced gap states (MIGS), defect-related states, and disorder-induced gap states (DIGS).[62] Although these states are classified according to their different structural origins, they are fundamentally caused by chemical interactions on the contact. Considering an additional interface dipole ($e\Delta_{dip}$), which is attributed to charge relaxation at the MSJ, the SBH is modified from the Schottky–Mott model to:

$$\Phi_{B,n} = \phi_M - \chi_S + e\Delta_{dip}, \quad \Phi_{B,p} = I_S - \phi_M - e\Delta_{dip} \quad (2)$$

$$e\Delta_{dip} = \int_{z_1}^{z_2}\iint z\Delta\rho(x,y,z)\mathrm{d}x\mathrm{d}y/S \quad (3)$$

where $z$, $\Delta\rho$, and $S$ are the coordinates normal to the surface, change in the charge density, and surface area, respectively.[60] The schematic MSJ band diagram, which is modified with various gap states and the interface dipole, is shown in Fig. 5a. Unfortunately, the interface dipole cannot be clearly determined due to the ambiguity of the contributors and bulk states.[62,63] The linearly fitted slope of the $\Phi_B$-versus-$\phi_M$ plot is deduced as a measure of the FLP strength, so-called interface behavior parameter, or $S$ parameter of the semiconductor ($S_\Phi$).[62,64]

$$S_\Phi \equiv \left|\frac{\partial\Phi_B}{\partial\phi_M}\right| = \left|1 + \frac{e\partial\Delta_{dip}}{\partial\phi_M}\right| \quad (4)$$

$S_\Phi$ = 1 indicates no pinning. From the experiments, $S_\Phi$ was determined to be 0.1 for the $MoS_2$-3D metal electrode (Sc, Ti, Ni, and Pt) junction, approximately 0.25 for GaSe, and 0.05 for n-Ge (Fig. 5b).[65] These small $S_\Phi$ values indicate a weak dependence of SBH on the work function; therefore, in a strong pinning situation, it becomes challenging to achieve SB-free MSJ even if the work function has been largely adjusted.

To avoid lattice mismatch-induced gap states (or DIGS) and MIGS, it is necessary to form TMD and MXene 2D contacts by secondary bonding. The atomically flat and defect-free MSJ, which is difficult to achieve in 3D materials, can be easily achieved with 2D metals and 2D semiconductors *via* their chemically saturated surfaces, consequently suppressing defect-related states. More than 70 MXenes are theoretically expected to afford optimized coupling between MXenes and TMDs. Some recent studies have demonstrated the feasibility of constructing SB-free contacts with black phosphorus, $MoS_2$, and GaN.[11b–d] Liu *et al.* investigated the electronic state of T-$MoS_2$-H-$MoS_2$ as an example of a 2D-metal–2D-semiconductor *via* DFT calculations and found that the MSJ states originate from the metal rather than the semiconductor, leading to negligible

 

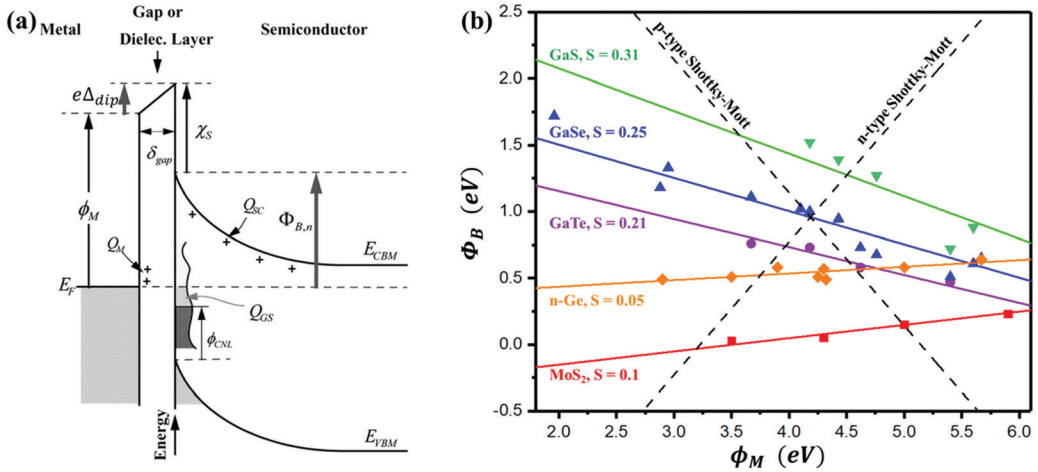


Fig. 5 (a) The fixed separation model for SBH formation. Electronic states, with a charge neutrality level (CNL) and density of states, were assumed to reside on the semiconductor surface, which is held at a fixed distance from the metal. Reproduced with permission.[62] Copyright 2014 AIP Publishing LLC. (b) SBH *versus* the contact 3D metal work functions for p-type GaS, GaSe, and GaTe, and n-type n-Ge, and $MoS_2$.[65] The solid and dotted lines represent a linear fit to the experimental points and the ideal Schottky–Mott limits with $S$ = 1, respectively.

MIGS in the junction (Fig. 6a).[64b] This is in contrast to the significant MIGS determined in the case of a 3D-metal–2D-semiconductor. The bond distance of T-$MoS_2$–H-$MoS_2$ was calculated to be within 3–4 Å, indicating typical vdW interactions, where the vdW interactions were not strong enough to induce MIGS. The suppression of MIGS in the semiconductor can therefore lead to a weak FLP, which was supported by the calculated $S_\Phi \cong 1$ for H-$MoS_2$–2D metals (Fig. 6b).

You *et al.* verified the HER activity of $MoS_2$ with seven representative O-terminated MXenes ($V_2CO_2$, $Cr_2CO_2$, $Mo_2CO_2$, $Ti_3C_2O_2$, $V_4C_3O_2$, $Cr_2NO_2$, and $V_2NO_2$), which were used in p-type SB-free contacts with near-zero SBH from −0.185 to +0.245 eV.[11a] The report suggests that the metallic properties of 2H-$MoS_2$, induced by the SB-free contact at the interface of $MoS_2$/MXenes, enhance the hydrogen adsorption ability on the basal plane of 2H-$MoS_2$, based on an analysis of the hydrogen adsorption energy ($\Delta E_H$) of the heterostructure of $MoS_2$ with O-terminated MXenes. In more detail, when MXenes with near-zero SBH were contacted with semiconducting 2H-$MoS_2$, the Fermi level of the MXenes was located at or below the valence band maximum of 2H-$MoS_2$, which could result in metallic properties of 2H-$MoS_2$. Therefore, these SB-free p-type 2H-$MoS_2$/MXenes exhibited enhanced charge transfer kinetics for the HER. As shown in Fig. 7a, the $\Delta E_H$ of the 2H-$MoS_2$/MXenes was considerably lower than that of pristine 2H-$MoS_2$, reaching values comparable to that of 1T-$MoS_2$. This could result in dramatically improved H adsorption on the basal plane of 2H-$MoS_2$ in 2H-$MoS_2$/MXene hybrids. Furthermore, the adsorption of H on the S vacant sites seemed to be strengthened; $\Delta E_H$ for a single S vacancy on the basal plane of 2H-$MoS_2$/$Cr_2CO_2$ was −3.08 eV, while that of the pristine $MoS_2$ was −2.06 eV.

Another important characteristic of the TMD/MXene hybrids relates to the ion diffusion rate and capacity for energy storage applications. The flexibility of the vdW interaction of 2D TMD/MXenes allows the reversible intercalation of guest ions without significant destruction of the layers. Tang *et al.* recently predicted that proper combinations of $MoS_2$ and $VS_2$ with Mo-, Nb-, Ti-, and V-based-MXenes could be effective for application in Na-ion batteries, based on DFT calculations.[66] First, the study revealed that the interaction between TMDs and bare MXenes was stronger compared to that with O-terminated MXenes, suggesting more potent cohesive energies for the former. All these cohesive energies were negative, which suggests that the construction of stacked TMDs with MXenes is an exothermic reaction. Second, O-terminated MXenes showed a better capacity for intercalating five layers of $Na^+$ ions (Fig. 7b) without severe structural distortion due to their large interlayer space (2.59–2.81 Å), compared to those of bare MXenes and TMDs (1.62–2.40 Å). Furthermore, the minimal barriers for layer-to-layer $Na^+$ diffusion (0.091–0.371 eV for $MoS_2$ and 0.097–0.221 eV for $VS_2$) were sufficient to facilitate fast charge/discharge processes. Considering the optimal adsorption sites of the TMD/MXene structure for $Na^+$ ions, five layers of $Na^+$ ions could be formed around the TMD/MXenes. The $MoS_2$/O-terminated MXenes behaved differently from $VS_2$/O-terminated MXenes; some of the $Na^+$ ions escaped from the S-terminated surfaces of $MoS_2$, whereas no such phenomenon was observed for the latter. On the basis of the above results and by visualizing the electron localization functions (ELFs) along the (110) plane of $VS_2$ with O-terminated MXenes, they concluded that $VS_2$ with an O-terminated $Ti_2CO_2$ structure could accommodate five layers of $Na^+$ ions without severe structural distortion upon intercalation of the $Na^+$ ions, with rapid charge/discharge processes.

## 4. Synthesis of TMD decorated MXenes

In recent years, several MXene-TMD composite structures have been reported for various electrochemical applications. The

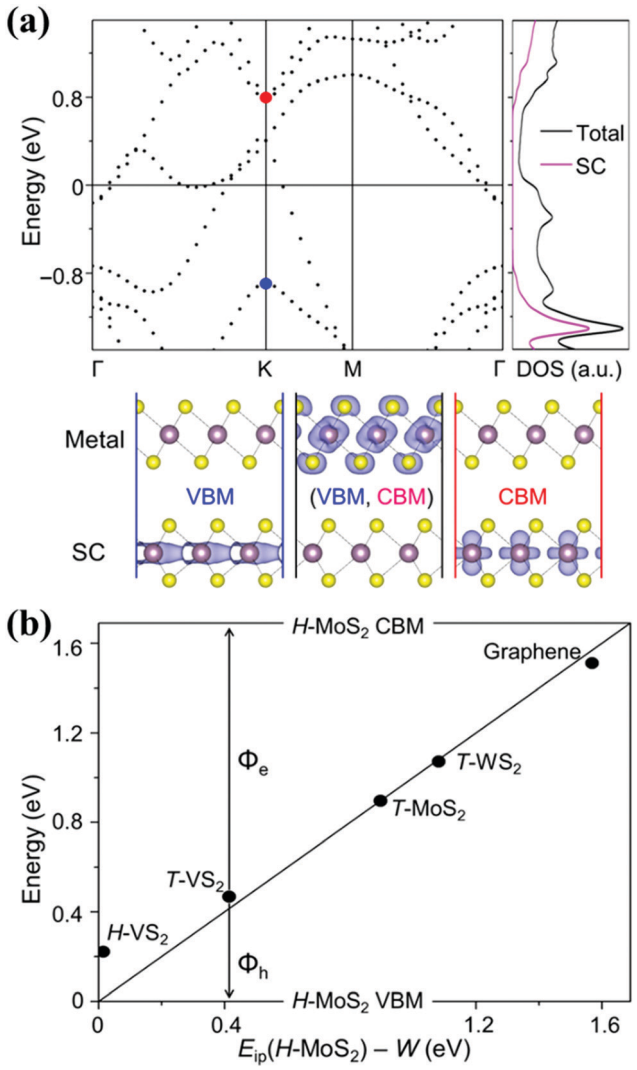


Fig. 6 (a) Electronic band structure and density of states (DOS) of a typical vdW MSJ of metallic T-$MoS_2$ and semiconductor (SC) H-$MoS_2$. FL is set to zero. The VBM and CBM of the SC are marked by blue and red dots, respectively. Isosurfaces show the spatial distributions of the states. (b) SBH *versus* the contact 2D metal work functions. The diagonal line shows the ideal Schottky–Mott limit. Reproduced with permission.[64b] Copyright 2016, American Association for the Advancement of Science.

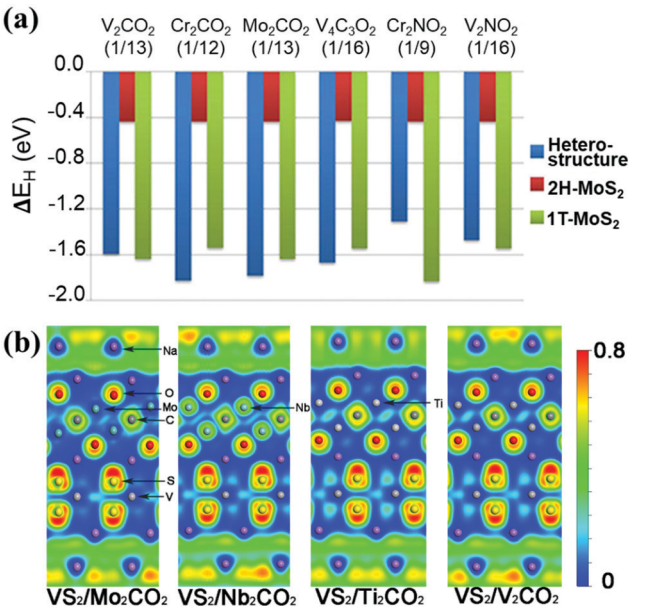


Fig. 7 (a) The plot of hydrogen adsorption energies ($\Delta E_H$) of 2H-$MoS_2$, 1T-$MoS_2$, and 2H-$MoS_2$/MXene heterostructures. Reproduced with permission.[11a] Copyright 2019, American Chemical Society. (b) Electron localization functions for the cross section of the (110) plane of $VS_2/Mo_2CO_2$, $VS_2/Nb_2CO_2$, $VS_2/Ti_2CO_2$, and $VS_2/V_2CO_2$, respectively, with five layers of $Na^+$ ions. Reproduced with permission.[66] Copyright 2019, American Chemical Society.

combination of MXene–TMDs forms an open structure in which the stacking issue affecting the individual materials can be resolved, thus maintaining the interlayer space and resulting in fast ion transfer between the sheets, which makes these composites promising and desirable electrode materials. The recent development of various TMD/MXene composite nanostructures is presented in the following subsections (Fig. 8).

### 4.1. $MoS_2$–MXene

Among the transition metal dichalcogenides, $MoS_2$ (bulk and delaminated forms) has been established as a versatile and prominent material for dry lubrication, catalysis, biological, electrochemical, and electronics applications.[67] Thin 2D $MoS_2$ affords great electrochemical performance because of its catalytically active edges, layered dynamic morphology, hydrophilicity, and tunable bandwidth.[56a,68] Thus, $MoS_2$ has gained immense interest for electrochemical applications, and its performance is comparable to that of graphene and carbon nanotube electrodes.[56d,69] However, the significant constraints of $MoS_2$ include its low intrinsic conductivity, inadequate active sites, oxidation of the edges, limited voltage window, structural disintegration, and poor cycling stability.[68,70] To address these issues, $MoS_2$-based composites such as $MoS_2$–graphene/CNT/$Fe_3O_4$ hybrid structures have been synthesized, but moderate conductivity and volume expansion still remain major challenges.[71] Two-dimensional MXenes have been proven to be efficient electrode materials owing to their superior metallic conductivity and hydrophilicity combined with cyclability. Therefore, MXene-based $MoS_2$ hybrid composites have been extensively explored to overcome the above limitations.[71b] $Ti_3C_2$ is typically used as a representative MXene material for the synthesis of TMD/MXene-based nanocomposites. A simple sintering method was first introduced by Shen *et al.*, where $MoS_2$@$Ti_3C_2$ nanocomposite powder was obtained *via* a solid-phase sintering method using $Ti_3C_2$ as a starting material.[72] The hydrothermal method was also applied by Li *et al.* to form a TMD/MXene hybrid, where *in situ* uniform growth of $MoS_2$ nanolayers was achieved on the surface of $Ti_3C_2$.[57b] However, the synthesis of vertically aligned $MoS_2$ on a $Ti_3C_2$ support by a hydrothermal process, in the absence of carbon nano-plating, would readily oxidize $Ti_3C_2$ to $TiO_2$ and lead to structural degradation.[73] Consequently, Attanayake *et al.* reported that the exposure of a colloidal solution of exfoliated $Ti_3C_2$ and $(NH_4)_2MoS_4$ to microwaves at a specific temperature generated sufficient heat for the nucleation and perpendicular growth of $MoS_2$ on the $Ti_3C_2$ surface. The resulting $MoS_2$

 

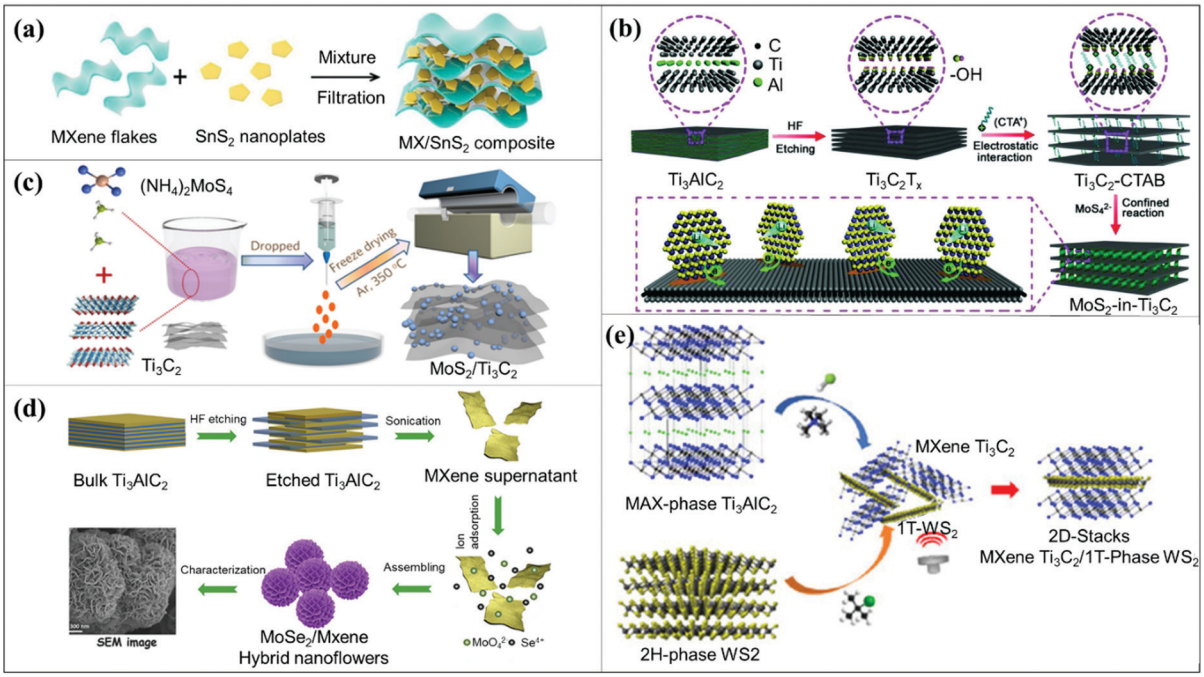


Fig. 8 Various approaches for the synthesis of TMD-MXene hybrid structures. (a) Synthesis of a $SnS_2$–MXene composite by sonication and vacuum-assisted filtration through a polypropylene membrane. Reproduced with permission.[6] Copyright 2018, Elsevier. (b) Synthesis of the $MoS_2$-in-$Ti_3C_2$ ($MoS_2$-out-$Ti_3C_2$) hybrids by electrostatic attraction in the presence (absence) of cetyltrimethyl ammonium bromide. Reproduced with permission.[75] Copyright 2018, Wiley. (c) Synthesis of $MoS_2/Ti_3C_2$ hybrid material prepared *via* freeze-drying followed by thermal decomposition. Reproduced with permission.[71b] Copyright 2020, Wiley. (d) Step-by-step synthesis of $MoSe_2$/MXene hybrid nanoflowers by a simple hydrothermal method; inset picture shows the SEM image of $MoSe_2$/MXene hybrid nanoflowers. Reproduced with permission.[82] Copyright 2020, Elsevier. (e) Schematic illustration of introduction of 1T-$WS_2$ between the delaminated matrixes of $Ti_3C_2$ through a simple sonication process to produce a 2D $Ti_3C_2$/1T-$WS_2$ hybrid structure. Reproduced with permission.[10] Copyright 2019, Wiley.

nanosheets were vertically oriented on the $Ti_3C_2$ support.[74] Ma *et al.* and Chen *et al.*, respectively, reported other techniques, including electrostatic interaction and laser engraving-assisted fabrication for the formation of $MoS_2$–$Ti_3C_2$ nanocomposites.[58e,75] Other MXenes such as $Mo_2CT_x$ (T = O-, OH-, or F-terminated groups), $V_4C_3$, and $Mo_2TiC_2T_x$ have also been successfully coupled to $MoS_2$ (Fig. 9a–d).[76]

### 4.2. $WS_2$–MXene

$WS_2$ is also a naturally occurring layered TMD, and exfoliated $WS_2$ shows impressive optical and electrochemical/catalytic properties,[77] making it amenable to diverse applications.[78] The space present between the sheets of $WS_2$ allows for intercalation of atoms, forming high-efficiency materials for energy storage applications.[79] To overcome the intrinsically low electrical conductivity, poor rate capability, low cycling stability, and massive volume expansion of $WS_2$, significant efforts have been devoted to fabricating hybrid $WS_2$-based nanostructures.[80] The $WS_2$–$Ti_3C_2$ nanohybrid structure has been easily synthesized due to the abundant nucleation sites provided by $Ti_3C_2$ for the growth of $WS_2$; Su *et al.* introduced the vapor phase deposition of $WS_2$ flakes over $Ti_3C_2T_x$.[81] The report suggests that the desired layers of $WS_2$ flakes can be achieved simply by controlling the growth parameters. Vyskočil *et al.* reported the synthesis of 2D nanohybrids by sonication of delaminated $Ti_3C_2$ ($Ti_3C_2$-D), prepared using tetrabutylammonium hydroxide, with different ratios of 1T-phase $WS_2$ nanolayers.[10] The multilayer stacking arrangement of $Ti_3C_2$-D and 1T-phase $WS_2$ was confirmed through transmission electron microscopy (TEM) imaging. The ideal ratio of delaminated $Ti_3C_2$ to 1T-phase $WS_2$ was noted to be 90 : 10 by comparing the capacitance for different ratios of 1T-phase $WS_2$.

### 4.3. Other TMD/MXenes

In addition to $MoS_2$ and $WS_2$, other TMD/MXene-based composites with $MoSe_2$, $SnS_2$, and $WSe_2$ have been reported. For example, a $MoSe_2$–MXene composite (Fig. 9e and f) was developed by employing a hydrothermal approach followed by annealing.[57a,82] The $MoO_4^{2-}$ and $Se^{4+}$ ions formed were adsorbed on the surface of ultrasonicated $Ti_3C_2$, resulting in the formation of a 3D $MoSe_2$–$Ti_3C_2$ hybrid nanoflower-like structure. On the other hand, Li *et al.* prepared 1T/2H-$MoSe_2$/MXene catalysts *via* a simple hydrothermal method, where $Na_2MoO_4$, Se powder, and $NaBH_4$ were dispersed in DI water with as-prepared $Ti_3C_2$ MXene nanosheets.[83] This solution was heated in a steel autoclave at 220 °C for 20 h to produce 1T/2H-$MoSe_2$/MXene. They revealed the existence of 1T- and 2H-$MoSe_2$ from the lattice fringes using HRTEM, visualizing the characteristic atomic arrangement of 1T- and 2H-$MoSe_2$ on the (002) plane, where trigonal and honeycomb atomic arrangements were observed for the 1T and 2H phases, respectively. Raman analysis further showed that the 1T and 2H phases of $MoSe_2$ coexisted in 1T/2H-$MoSe_2$/MXene; the two typical Raman peaks of

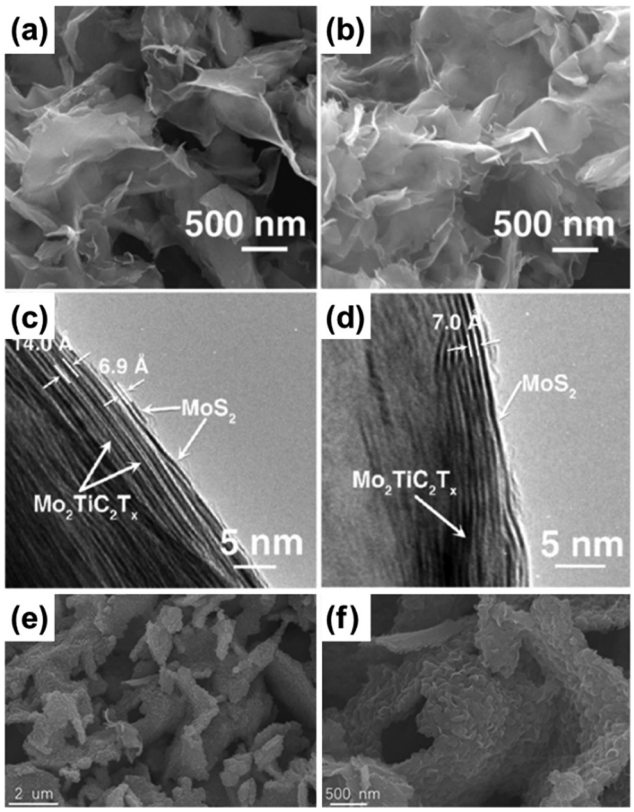


Fig. 9 (a) and (b) SEM images of $MoS_2/Mo_2TiC_2T_x$ heterostructures at 500 °C and 700 °C, respectively. (c) and (d) Cross-sectional TEM images of $MoS_2/Mo_2TiC_2T_x$ heterostructures at 500 °C and 700 °C, respectively, indicate 2D layers with $MoS_2$ on $Mo_2TiC_2T_x$. Reproduced with permission.[76c] Copyright 2018, Wiley. (e) and (f) FESEM images of $MoSe_2/Ti_3C_2$ heterostructures at various magnification. Reproduced with permission.[57a] Copyright 2020, Elsevier.

2H-$MoSe_2$/MXene were observed at 241 ($A_{1g}$) and 285 $cm^{-1}$ ($E_{2g}{}^1$), while the profile of 1T/2H-$MoSe_2$/MXene exhibited not only negatively shifted Raman peaks (5–6 $cm^{-1}$) for the $A_{1g}$ and $E_{2g}{}^1$ states, but also two additional peaks at 195 and 350 $cm^{-1}$, which were not observed in the Raman spectra of 2H-$MoSe_2$/MXene and MXene. However, the exact ratio between the 1T and 2H phases was not reported.

The synthesis of $SnS_2$–MXene composites was reported by Wu *et al.*, where the composite was synthesized by mixing a colloidal solution of $Ti_3C_2T_x$ with $SnS_2$ solution at different mass ratios.[6] The heterostructure of $SnS_2$–$Ti_3C_2T_x$ was obtained after vacuum-assisted filtration of the aqueous mixture through a polypropylene membrane. Furthermore, Xu *et al.* (first report on TMD/MXene composites) reported the stacking of mechanically exfoliated $Ti_2C(OH)_xF_y$ flakes on the targeted $WSe_2$ flakes by a mechanical transfer method to fabricate $WSe_2$–$Ti_2C(OH)_xF_y$ heterostructures.[84]

# 5. Applications towards energy storage and conversion devices

As mentioned earlier, MXenes have high electrical conductivity, and their work function can be modulated by adjusting the layer thickness or surface termination. The ability to create a vdW heterointerface with TMDs, avoiding FLP, opens a door for applying hybrids of TMDs and MXenes in various fields such as energy conversion, energy storage, photo- and electrocatalysis, and optics.

## 5.1 Batteries and supercapacitors

Rechargeable batteries are considered a primary tool for energy storage. Thus, various nanomaterials have been explored and developed for fabricating high-performance energy storage materials.[85] Lithium-ion batteries are of great interest because of their compact, efficient storage mechanism and robust nature, which allow the shuttling of $Li^+$ ions between the anode (mostly graphite) and cathode (mostly lithium metal oxide).[86] Over the past decade, graphene-like layered 2D materials have been vastly investigated as electrode materials because of their large surface area, which can provide high capacity, combined with structural permanence.[87] As electrode materials in Li-ion batteries, graphene and transition metal oxide materials demonstrated superior and comparable capacity (744 and 700 mA h $g^{-1}$, respectively), with good cyclic stability.[88] Layered 2D TMDs display low volume change and possess numerous active sites due to their large surface area, making them different from the bulk counterparts; thus, these materials have attracted tremendous interest as electrode materials.[52]

Several studies have investigated 2D $MoS_2$ as an anode material for Li-ion batteries. The results revealed that exfoliated $MoS_2$ affords increased specific capacity (approximately 1131 mA h $g^{-1}$) and higher coulombic efficiency than the pristine $MoS_2$ electrode because the slack exfoliated $MoS_2$ layers can accommodate the volume variation.[89] Owing to the lack of structural integrity of the anode during the lithiation process and capacity reduction after several cycles, the construction of $MoS_2$-based composite electrodes has been highlighted. $MoS_2$@$TiO_2$ hybrid nanostructures prepared by Xu and co-workers afforded substantially improved specific capacity and rate capability.[90] Chang *et al.* effectively fabricated $MoS_2$/graphene nanosheet layered composites, which exhibited exceptionally high specific capacity and current density (1300 mA h $g^{-1}$ at 100 mA $g^{-1}$ and 1040 mA h $g^{-1}$ at 1000 mA $g^{-1}$).[56c] Similarly, as electrode materials, a composite of $MoS_2$ with $SnO_2$ and a CNT-supported $MoS_2$ nanohybrid afforded improved structural integrity with a long cycle life and high rate capability in Li-ion batteries.[91] In $MoS_2$–carbon-based electrodes, the presence of carbon sites led to numerous side reactions, which reduced the overall efficiency.[71b]

2D MXene ($Ti_3C_2$)-based electrodes exhibit an attractive reversible volumetric capacitance (1375 mA h $cm^{-3}$), which is twice that of the graphite electrode (550 mA h $cm^{-3}$), because of the excellent electrochemical properties of the former.[92] By exploiting the properties of layered MXenes, Hu *et al.* and Du *et al.* reported the synthesis of a $MoS_2/Ti_3C_2T_x$ hybrid composite as an anode material for Li-ion batteries.[71b,93] The resulting $MoS_2/Ti_3C_2T_x$ composite delivered a stable reversible capacitance (614.4 mA h $g^{-1}$ at 100 mA $g^{-1}$) with low electrochemical impedance and better rate performance (Fig. 10a and b). This performance was mainly attributed to the unique structure and

 

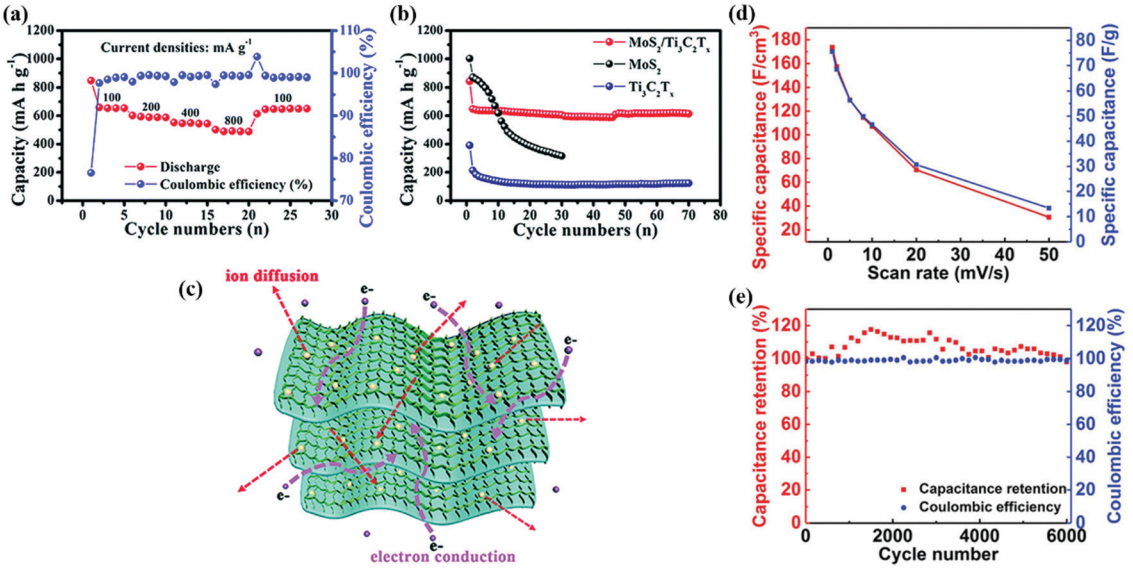


Fig. 10 (a) Rate performance of the $MoS_2/Ti_3C_2T_x$ composite for different discharge capacities with coulombic efficiency almost 100%. (b) Cycling stability of the $MoS_2/Ti_3C_2T_x$ composite compared to $MoS_2$ and $Ti_3C_2T_x$. (c) Schematic representation of $MoS_2$ layers uniformly distributed over $Ti_3C_2T_x$, along with the ion diffusion and electron conduction paths. Reproduced with permission.[93] Copyright 2019, The Royal Society of Chemistry. (d) Specific capacitance of a micro supercapacitor (MXene-$MoS_2$) at different scan rates. (e) Capacitive retentivity and coulombic efficiency of a micro supercapacitor. Reproduced with permission.[58e] Copyright 2019, Wiley.

synergistic effect, which hindered the agglomeration and volume expansion of the $MoS_2$ nanosheets due to the large conductive surface of the $Ti_3C_2T_x$ substrate (Fig. 10c), which promoted rapid electron/$Li^+$ transfer kinetics. Similarly, Wu *et al.* assembled $MoS_2$/$Ti_3C_2$–MXene@C nanohybrids as anodes and evaluated their utility in lithium batteries using CR2016 coin cells, which had an ideal mass loading of electrodes of approximately 0.8–1.0 mg $cm^{-2}$. The test demonstrated high capacity and prolonged cycle life (3000 cycles) at a high current density.[73] This significant improvement was due to the reduced number of pathways for mass and charge diffusion from the $MoS_2$ nanostructures, along with the carbon nanoplating, which improved the electronic coupling between the $MoS_2$ nanostructures with $Ti_3C_2$ and also provided structural stability.

On the other hand, $V_4C_3$ exhibited better structural durability and specific capacity as an anode material than $Ti_3C_2$.[76a] Considering this, Bai and co-workers produced a $V_4C_3/MoS_2$/C nanohybrid for a high-rate Li-ion battery, which displayed a high specific capacitance at high current rates (622.6 and 500 mA h $g^{-1}$ at 1 and 10 A $g^{-1}$, respectively), and enhanced cycling efficiency in the potential range of 0.01–3.0 V (*vs.* $Li/Li^+$), with an optimal mass loading of 1–2 mg $cm^{-2}$. The improved electrochemical performance resulted from the increased electrical conductivity and structural stability due to $V_4C_3$ and the thin carbon coating, while the $MoS_2$ nanosheets led to higher specific capacitance and enhanced charge mobility. Because sodium-ion batteries are regarded as a cheaper alternative to Li-ion batteries, extensive studies have been dedicated to identifying an optimum anode material for these batteries.[94] With respect to this, Wu *et al.* reported $MoS_2/Ti_3C_2T_x$ composites synthesized by the hydrothermal method as an anode material for Na-ion batteries.[11g] The evaluation of the electrochemical properties of the $MoS_2/Ti_3C_2T_x$ composite using a CR2032 coin-type cell with Na–metal as the counter-electrode, within the voltage window of 0.01–3.0 V (*vs.* $Na/Na^+$), demonstrated the excellent reversible capacity (250.9 mA h $g^{-1}$ at 100 mA $g^{-1}$), high cycling stability, and rate capability, attributed to the nested architecture of the composite. While the $MoS_2$ nanosheets increased the capacity of the composite, the presence of $Ti_3C_2T_x$ favored the open structure, and the decreased concentration of fluorine on the surface afforded improved electrochemical performance of the composite. The weak van der Waals forces of $MoS_2$ and the large interlayer spaces of MXene, capable of accommodating various cations (such as $Na^+$, $K^+$, $NH^{4+}$, $Mg^{2+}$, and $Al^{3+}$), have attracted great interest for the use of these materials in non-lithium batteries.[56a,95] Inspired by this, the possibility of using $MoS_2$–MXene composite electrodes in magnesium, potassium, and lithium–sulfur batteries has been explored.[57b,96] Electrochemical measurements displayed superior reversible capacity, remarkable rate performance, and cycling durability. However, research on $MoS_2$–MXene composites for non-lithium batteries is still at an early stage, calling for further study.

Seo *et al.* and Sun *et al.* reported $SnS_2$ as an electrode material for Li-ion and Na-ion batteries, respectively, and achieved exceptional specific capacity, rate performance, and cyclability.[97] To overcome the inherent constraints of $SnS_2$, such as tremendous volume change and large capacity fading in Na-ion batteries, Wu and co-workers subjected the $Ti_3C_2T_x$/$SnS_2$ heterostructure (mass ratio MXene/$SnS_2$ = 1 : 5) to charge/discharge tests within the potential range of 0.01–2.5 V (*vs.* $Na/Na^+$) using LAND 2001A. They demonstrated that the specific capacity was maintained, even at high temperatures, when used as an anode material.[6] Li *et al.* prepared a $Ti_3C_2T_x$-decorated

$SnS_2/Sn_3S_4$ hybrid *via* a solvothermal process and examined the resultant composite as an anode for Li-ion batteries, within the voltage range of 0.005–3.0 V, at room temperature.[11e] Interestingly, the composite displayed steady cycling performance, with notable rate capability, attributed to expeditious electron transfer with little volume variation. Furthermore, the increased surface interaction between the electrode and electrolyte due to the large specific area of $SnS_2/Sn_3S_4$ led to partial pseudocapacitance at high current densities, thereby increasing the $Li^+$ ion diffusion. Li and co-workers recently studied a $MoSe_2$/MXene heterojunction for Na-ion batteries, with an average electrode loading mass of approximately 1.1 mg $cm^{-2}$. The battery could maintain reversible capacity at a high current density and exhibited promising electrochemical qualities.[57a] The mechanism of rapid $Na^+$ ion shuttling and the better electronic structure of $MoSe_2$/MXene were confirmed theoretically (density-functional theory calculations) and experimentally (galvanostatic intermittent titration and electrochemical impedance spectroscopy).

Supercapacitors belong to a class of electrochemical energy storage devices and can deliver higher power densities quickly with protracted charge/discharge cycles compared to batteries.[98] Graphene is considered one of the best-suited materials for supercapacitors owing to its high surface area, excellent conductivity, intrinsic stability, and high volumetric capacitance (376 F $cm^{-3}$).[99] However, during charging and discharging, these materials undesirably undergo layer restacking, which decreases the charge storage due to the restricted availability of the surface area. The use of hydrous ruthenium oxide in pseudocapacitors afforded impressive supercapacitance ($\sim$900 F $g^{-1}$) and cycling efficiency. However, when the water content was reduced, the capacitance also decreased (to 29 F $g^{-1}$).[100] On the other hand, MXenes combine large surface areas with superior hydrophilicity and conductivity and provide significantly high capacitance, exceeding that of the best-known carbon supercapacitor.[14b] Ghidiu *et al.* first introduced a new, safe, and easy protocol for the synthesis of additive-free clay-like MXenes and provided a faster approach for obtaining delaminated flakes.[15] When these clay-like MXenes were rolled into thin sheets for supercapacitor electrodes, they displayed remarkable volumetric capacitance of up to 900 F $cm^{-3}$ and better rate-handling ability. However, the aggregation of the layers inhibited the complete utilization of MXene, which hindered ion transport and strongly reduced the capacity. Acerce and co-workers showed that metallic 1T-phase $MoS_2$ nanosheets can be chemically exfoliated to facilitate the intercalation of various cations ($H^+$, $Li^+$, $Na^+$, and $K^+$), leading to high capacitance ($\sim$400–700 F $cm^{-3}$) with excellent cycling stability (about 5000 cycles) in both aqueous and organic electrolytes.[56a] The ability of the exfoliated layers to expand, along with the high hydrophilicity and electrical conductivity (nearly $10^7$ times higher than those of the semiconducting 2H phase) of the 1T $MoS_2$ phase, resulted in excellent electrochemical properties. By introducing $MoS_2$ between the MXene sheets, the intrinsic drawbacks of both materials can be eliminated, thereby enhancing the electrochemical performance. Only recently, the 1T-phase $WS_2/Ti_3C_2$ nanohybrid was studied, where a high capacitance (157 F $g^{-1}$) was observed for 90% $Ti_3C_2$/10% 1T-phase $WS_2$, and no improvement was observed upon further addition of 1T-phase $WS_2$.[10] The study discussed the increase in the capacitance for each step of exfoliation of $Ti_3C_2$, where a substantial increase (nearly 59%) was observed upon inserting $WS_2$ due to the larger exposed surface area. The enhanced capacitance of the nanohybrid was comparable to that of other hybrid materials. Designing an efficient microsupercapacitor is crucial for portable and wearable electronics. Recently, Chen *et al.* synthesized a $Ti_3C_2T_x$–$MoS_2$ film by direct laser etching and evaluated the results for a microsupercapacitor.[58e] The composite afforded a significantly high specific capacitance (173.6 F $cm^{-3}$, which is 60% more than that of pristine MXene), good coulombic efficiency (around 98%), and longer cycling rates (approximately 6000) (Fig. 10d and e). The study also demonstrated the great flexibility of the hybrid electrode, wherein 89% of the capacitance was retained when the electrode was bent at an angle of 150°.

Although the majority of the research has focused on developing MXene–TMD heterostructures for lithium batteries, MXene–TMD heterostructures have also displayed promising results as functional materials for non-lithium batteries. Among the large families of MXene and TMD materials, $Ti_3C_2T_x$ and $MoS_2$ have been the forerunners. However, the successful reversible transformation of $MoS_2$ from $LiS_2$ during discharging and charge storage needs to be studied in detail. Significant focus needs to be placed on research for developing TMD-MXene composites for supercapacitor materials to further advance energy storage devices.

### 5.2 Electrochemical energy conversion

Among TMDs, molybdenum-and tungsten-based disulfides and diselenides are the most widely utilized electrocatalysts due to their excellent and efficient electrochemical catalytic performance in energy conversion applications, such as the hydrogen evolution reaction (HER), oxygen evolution reaction (OER), and oxygen reduction reaction (ORR).[9b,101] However, as mentioned in Section 3.1, one of the critical weaknesses of TMDs is the low conductivity of the 2H phase.[83] Therefore, the construction of a hybrid structure with highly conductive MXene is an ingenious solution that has been adopted to overcome the low electrical conductance of the 2H phase in electrochemical applications. According to a report by Attanyake *et al.*, $MoS_2$ nanosheets vertically grown on $Ti_3C_2$ nanosheets ($MoS_2 \perp Ti_3C_2$@240) were prepared at reaction temperatures of 200–260 °C.[74] The edge density of $MoS_2$ was controlled by the reaction temperature, and the highest density of $MoS_2$ edges was obtained at 240 °C due to the complete reduction of the $(NH_4)_2MoS_4$ precursor (Fig. 11a). Evaluation of the electrocatalytic HER performance of the composite showed that the HER activity of the $MoS_2 \perp Ti_3C_2$ catalysts was proportional to the edge density of $MoS_2$, as shown in Fig. 11b, and the optimal overpotential to drive the current density of 10 mA $cm^{-2}$ was 110 mV for $MoS_2 \perp Ti_3C_2$@240, with a Tafel slope of $\sim$40 mV $dec^{-1}$. Moreover, MXenes are known to be metastable due to their poor oxygen resistance under oxygen-rich conditions (even under ambient conditions).[102] As a result of the undesirable spontaneous oxidation, transformation to metal oxides has been reported for

 

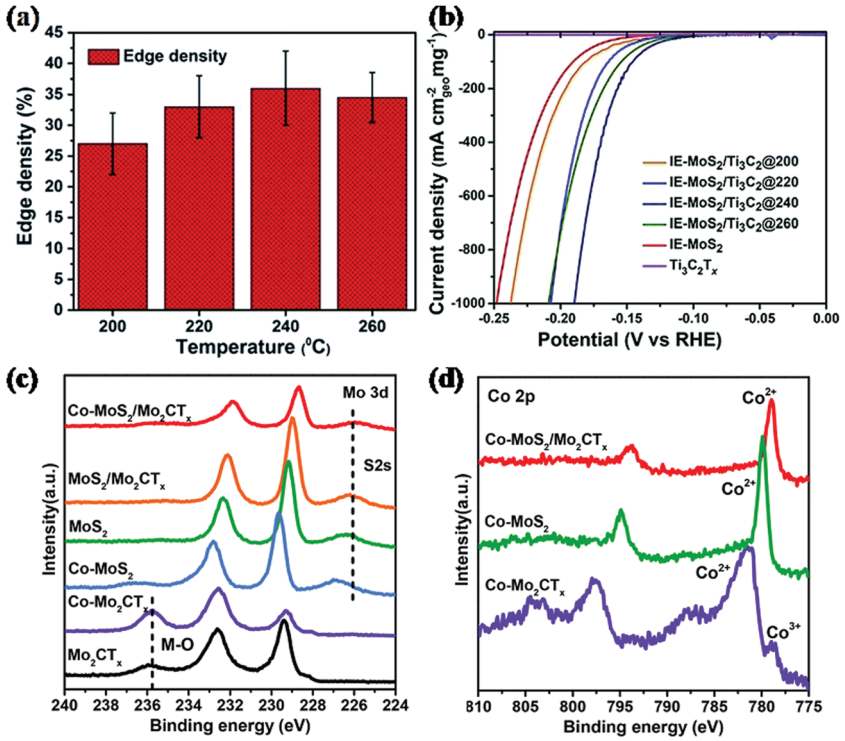


Fig. 11 (a) Edge density plots and (b) HER polarization plots in 0.5 M $H_2SO_4$ solution of IE-$MoS_2$/$Ti_3C_2$ sheets prepared at 200, 220, 240, and 240 °C. Reproduced with permission.[74] Copyright 2018, The Royal Society of Chemistry. X-ray photoelectron spectroscopy (XPS) spectra of (c) Mo 3d and (d) Co 2p of different materials. Reproduced with permission.[105b] Copyright 2019, The Royal Society of Chemistry.

several MXenes, leading to a decrease in the catalyst stability and activity.[103] Wu *et al.* reported carbon nano-plating as an effective strategy for constructing a $MoS_2$/$Ti_3C_2$ hybrid with improved HER stability and catalytic activity.[73] The surface of $Ti_3C_2$ MXene was protected by the carbonization of glucose by a facile hydrothermal method and subsequent annealing. The HER performance of $MoS_2$/$Ti_3C_2$–MXene@C in 0.5 M $H_2SO_4$ was compared to that of a hybrid of $MoS_2$ and oxidized $Ti_3C_2$ MXene ($MoS_2$@oxidized MXene) without carbon nano-plating. The overpotential at a current density of 10 mA $cm^{-2}$ ($\eta^{10}$) for $MoS_2$/$Ti_3C_2$–MXene@C was found to be 135 mV, whereas that of $MoS_2$@oxidized MXene was ~350 mV. The improved catalyst activity was attributed to the prevention of the direct exposure of MXene to the environment, where the charge transfer resistance ($R_{ct}$) of $MoS_2$/$Ti_3C_2$–MXene@C (39 Ω) was significantly lowered due to the carbon nano-plating, whereas the charge transfer resistance of $MoS_2$@oxidized MXene was 57 Ω. Additionally, $MoS_2$/$Ti_3C_2$–MXene@C showed better long-term stability of up to 2000 cycles, as demonstrated by chronoamperometric study at −130 mV for 20 h. Recently, Ren *et al.* reported a Mo-based MXene hybrid HER catalyst with $MoS_2$ nanoflowers ($MoS_2$@$Mo_2CT_x$) instead of Ti-based MXene. In 1.0 M KOH solution, the $\eta^{10}$ of $MoS_2$@$Mo_2CT_x$ was 176 mV, whereas the $\eta^{10}$ of $Mo_2CT_x$ and $MoS_2$ was 533 and 394 mV, respectively.[76b] This highly synergetic HER performance of $MoS_2$@$Mo_2CT_x$ could be achieved by the fast electron transport induced by the intrinsic conductivity of $Mo_2CT_x$ and the numerous exposed active sites for hydrogen adsorption on the $MoS_2$ nanoflowers. The electrochemical impedance of $MoS_2$@$Mo_2CT_x$ was only 26 Ω, compared to that of $MoS_2$ (660 Ω) and $Mo_2CT_x$ (155 Ω). The double-layer capacitance ($C_{dl}$), which is related to the electrochemically active surface area (ECSA) of $Mo_2CT_x$ (106 mF $cm^{-2}$) was the highest in $MoS_2$@$Mo_2CT_x$ (the $C_{dl}$ of $MoS_2$ and $Mo_2CT_x$ was 21.7 and 22.6 mF $cm^{-2}$, respectively). In contrast to the above examples, Lim *et al.* oxidized MXenes to prepare nanohybrids of 2H-$MoS_2$ on $Mo_2CT_x$ MXene for the HER *via in situ* sulfidation of an adventitious oxide layer on $Mo_2CT_x$.[104] $Mo_2CT_x$/2H-$MoS_2$ required an overpotential of only 119 mV to reach a current density of 10 mA $cm^{-2}$ in 0.5 M $H_2SO_4$ solution. They claimed that this exceptionally high HER activity originated from the epitaxially grown lattice interface between $Mo_2CT_x$ and 2H-$MoS_2$, where the oxidation layers were removed by sulfidation.

Furthermore, the optimized weight ratio of TMD to MXene and doping on the TMDs was suggested as a strategy for improving the electrochemical water splitting performance.[105] Huang *et al.* synthesized a series of weight ratio-controlled hierarchical 2H-$MoS_2$ nanosheets grown vertically on $Ti_3C_2$ MXenes ($MoS_2$/$Ti_3C_2$ heterostructures).[105a] The HER activity of the $MoS_2$/$Ti_3C_2$ heterostructures was demonstrated in 0.5 M $H_2SO_4$ electrolytes, and the overpotentials required to reach a current density of 10 mA $cm^{-2}$ were optimized for $MoS_2$/$Ti_3C_2$-5% (~280 mV), with a Tafel slope of 68 mV $dec^{-1}$. Although the exact values of the overpotentials of the other materials ($MoS_2$/$Ti_3C_2$-1%, -10%, and -20%) were not mentioned, the difference in the activity of the various catalysts could be distinguished from the

polarization plots. The enhanced HER activity of the $MoS_2$/$Ti_3C_2$-5% catalyst was associated with the strong interfacial coupling between $MoS_2$ and $Ti_3C_2$ at that component ratio, which resulted in enhanced charge transfer. Indeed, among the catalysts, the Tafel slope was the smallest for $MoS_2$/$Ti_3C_2$-5%; the Tafel slopes of $MoS_3$/$Ti_3C_2$-1%, -10%, and -20% were reported to be 109, 74, and 90 mV $dec^{-1}$, respectively. In addition, the increased number of active sites of $MoS_2$/$Ti_3C_2$-5% could afford an enhanced activity, as suggested by the larger $C_{dl}$ value (61.3 mF $cm^{-2}$) compared to that of the $MoS_3$/$Ti_3C_2$-1, -10, and -20% catalysts (41.3, 57.1, and 47.0 mF $cm^{-2}$, respectively). According to a recent report by Liang *et al.*, the Co-doped $MoS_2$ hybrid structure with $Mo_2CT_x$ MXene afforded enhanced alkaline HER performance.[105b] The study revealed that Co doping could modulate the electronic structure of $MoS_2$ to reduce the kinetic barrier during the water dissociation step, promoting $OH^-$ desorption, as reported in earlier work.[106] The $Mo_2CT_x$ MXene synergistically serves as a superior conductive support to promote charge transfer by strong coupling with Co-doped $MoS_2$.[105b] The Mo 3d XPS profile showed a negative shift in the binding energy peak of Co–$MoS_2$/$Mo_2CT_x$ (−0.5 eV) and $MoS_2$/$Mo_2CT_x$ (−0.2 eV) compared to that of pristine $MoS_2$ (the Mo $3d_{5/2}$ and $3d_{3/2}$ peaks were observed at 229.2 and 232.3 eV, respectively), indicating strong coupling between $MoS_2$ and $Mo_2CT_x$, and consequently efficient electron transfer from $Mo_2CT_x$ to $MoS_2$ (Fig. 11c). The −1.1 eV shift of the Co 2p peak of Co–$MoS_2$/$Mo_2CT_x$ relative to that of Co–$MoS_2$ suggests strong coupling between Co–$MoS_2$ and $Mo_2CT_x$ (Fig. 11d). The $\eta^{10}$ of Co–$MoS_2$/$Mo_2CT_x$ for the HER in 1.0 M KOH solution was 112 mV, while those of $MoS_2$, $Mo_2CT_x$, Co–$MoS_2$, Co–$Mo_2CT_x$, and $MoS_2$/$Mo_2CT_x$ were 345, 280, 215, 365, and 204 mV, respectively. Furthermore, the smallest Tafel slope of 82 mV $dec^{-1}$ and $R_{ct}$ of 50 Ω were obtained for Co–$MoS_2$/$Mo_2CT_x$, suggesting that Co doping of $MoS_2$ on $Mo_2CT_x$ MXene effectively enhanced the HER activity of the TMD/MXene hybrid by modulating the electronic structure and further improving the conductivity.

Despite the great achievements in the use of TMDs in electrochemical applications, relatively few examples of hybrid TMDs and MXenes have been reported for the OER, ORR, and $CO_2$RR. However, some strategies for improving the electrocatalytic OER and ORR performance have recently emerged.[83,107] Li *et al.* combined multiphasic 1T/2H-$MoSe_2$ nanosheets with $Ti_3C_2$ MXene nanosheets to construct active and stable bifunctional electrocatalysts for water splitting in alkaline solution.[83] The formation of such composites can be attributed to the intrinsic properties of $MoSe_2$; the 1T phase is metallic and metastable, while the 2H phase is semiconducting and thermodynamically stable. Thus, the mixed phase comprising 1T- and 2H-$MoSe_2$ may simultaneously afford enhanced HER activity and stability, and the introduction of MXene with high conductivity may enhance the catalytic activity, providing rapid charge transfer in the catalyst. The bifunctional 1T/2H-$MoSe_2$/MXene catalyst showed good electrocatalytic performance towards water splitting in 1.0 M KOH solution. The overpotentials of 1T/2H-$MoSe_2$/MXene to drive the current density of 10 mA $cm^{-2}$ were 95 mV (HER) and 340 mV (OER), respectively, while comparatively larger values were observed for 2H $MoSe_2$/MXene (123 mV (HER) and 380 mV (OER)). The Tafel slopes of 1T/2H-$MoSe_2$/MXene for the HER (91 mV $dec^{-1}$) and OER (90 mV $dec^{-1}$) were smaller than those of 2H-$MoSe_2$/MXene (111 mV $dec^{-1}$). Furthermore, the evaluation of the long-term stability for overall water splitting, determined by chronopotentiometry, demonstrated better stability, where the current density of ∼10 mA $cm^{-2}$ was maintained at 1.64 V for 50 h. The study reveals that mixing the 1T/2H phases effectively enhanced the electrocatalytic activity and stability for electrochemical water splitting. Pang *et al.* provided an interesting approach for fabricating TMD/MXene hybrids for the OER.[107b] Instead of constructing the hybrid structure by merging the existing TMD and MXene, the TMD/MXene-like structure was synthesized *via* a bottom-up approach (Fig. 12a). The obtained $M_2Q_2C$ compounds (M, Q, and X correspond to transition metals, chalcogenides, and carbon or nitrogen, respectively) presented good conductivity and enriched active sites. Using this approach, the authors generated $Nb_2Se_2C$ compounds *via* solid-state synthesis. Confirmation of the crystal structure by Rietveld refinement of the XRD pattern revealed that $Nb_2Se_2C$ was iso-structural with $Ta_2S_2C$ and belonged to the hexagonal crystal system ($P\bar{3}m1$ space group). In addition, the electronic band structures calculated using density functional theory (DFT) indicated that there was an apparent overlap between the conduction and valence bands, suggesting that $Nb_2Se_2C$ is a semi-metallic material. The electrocatalytic OER performance of $Nb_2Se_2C$ was tested in 1.0 M KOH electrolyte, and a current density of 10 mA $cm^{-2}$ was achieved at an overpotential of 321 mV, with a Tafel slope of 238 mV $dec^{-1}$, whereas $NbSe_2$ required an overpotential of 415 mV, with a Tafel slope of 329 mV $dec^{-1}$ (Fig. 12b). EIS analysis demonstrated that $Nb_2Se_2C$ (60.89 Ω) had smaller charge transfer resistance than $NbSe_2$ (184.3 Ω), $RuO_2$ (60.89 Ω), and $IrO_2$ (84.59 Ω). In addition, chronoamperometry indicated that $Nb_2Se_2C$ showed good long-term stability, where the current density of 10 mA $cm^{-2}$ was maintained (>98.0%) at 350 mV for 24 h. Recently, Yang *et al.* reported a TMD/MXene hybrid quantum dot (QD) structure with carbon nanotubes (CNTs) as an electrocatalyst for the ORR under alkaline conditions (Fig. 12c).[107a] The higher surface area of QD $MoS_2$ with exposed edge atoms relative to that of the nanosheets is believed to provide extra active sites. Hybrid multiwalled CNTs decorated with $MoS_2$ and $Ti_3C_2T_x$ QDs ($MoS_2$QDs@$Ti_3C_2T_x$QDs@MWCNTs), which interact with each other through van der Waals forces, were prepared by simple stoichiometric mixing in solution. The hybrid structure exhibited outstanding ORR activity; the half-wave potential was 0.75 V (*vs.* RHE) with a Tafel slope of ∼90 mV $dec^{-1}$, while that of commercial Pt/C was 0.80 V with a Tafel slope of 89 mV $dec^{-1}$ (Fig. 12d). However, the mass activity of the $MoS_2$QDs@$Ti_3C_2T_x$QDs@MWCNTs (∼27 A $g^{-1}$) at 0.35 V was somewhat smaller than that of Pt/C (∼36 A $g^{-1}$), requiring further optimization of the hybrid structure.

So far, studies on the TMD/MXene hybrid system have mainly focused on their inherent high catalytic activity. The strategy for enhancing electron transfer by the SB-free 2D contact with highly conductive MXene would stimulate new ideas for the next designs of catalysts. Despite the existing promising reports, the

 

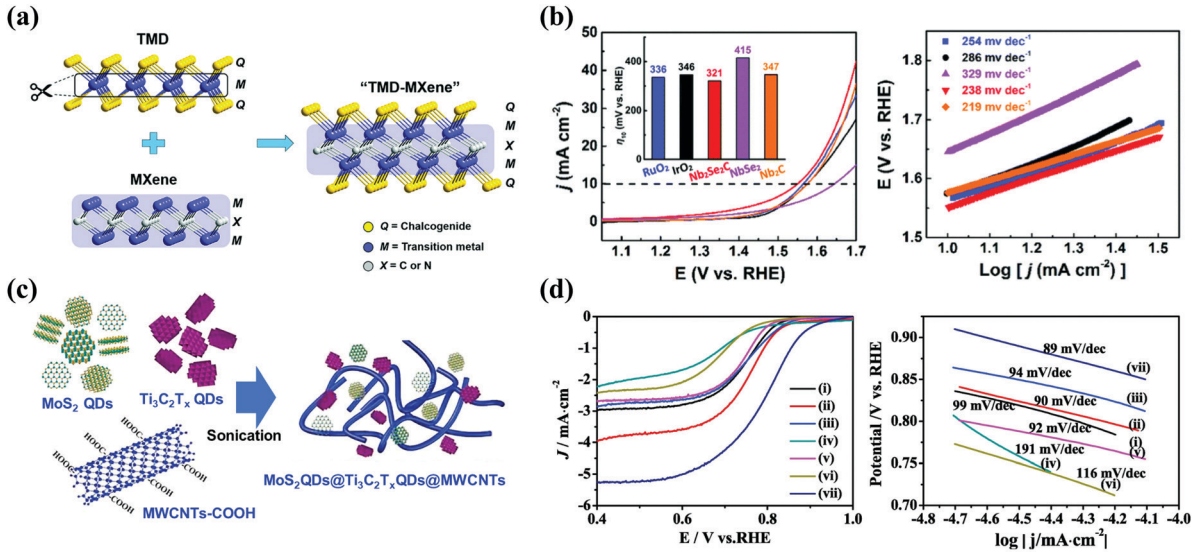


Fig. 12 (a) Schematic illustration of the concept for a "TMD-MXene"-like compound. (b) OER polarization curves in 0.1 M KOH solution (left) with the comparison of the overpotentials at 10 mA $cm^{-2}$ (inset) and Tafel plots (right) of $RuO_2$, $IrO_2$, $Nb_2Se_2C$, $NbSe_2$, and $Nb_2C$. Reproduced with permission.[107b] Copyright 2020, The Royal Society of Chemistry. (c) Schematic diagram of the preparation of $MoS_2$QDs@$Ti_3C_2T_x$QDs@MWCNTs. (d) ORR polarization curves in $O_2$-saturated 1.0 M KOH solution (left) and Tafel plots (right) of (i) $MoS_2$QDs@$Ti_3C_2T_x$QDs@MWCNTs-1, (ii) $MoS_2$QDs@$Ti_3C_2T_x$QDs@MWCNTs-2, (iii) $MoS_2$QDs@$Ti_3C_2T_x$QDs@MWCNTs-3, (iv) $Ti_3C_2T_x$ QDs, (v) MWCNTs, (vi) $MoS_2$ QDs, and (vii) Pt/C at 0.5 V. Reproduced with permission.[107a] Copyright 2019, Elsevier B.V.

catalytic stability of the TMD/MXene hybrids is still far from being satisfactory due to the poor oxygen resistance of MXene. Therefore, the efforts to enhance the oxidation stability of MXene or to explore less oxidative catalysis should be exerted in the future works.

## 6. Summary and outlook

The development of 2D materials has received substantial attention because of the outstanding physical and electrical properties of these materials. Atomic flat sheets without defects could be laminated by secondary bonding, providing flexibility and wide inter-sheet space, allowing facile ion intercalation and extraction without destroying the structures. Properties such as the electrical carrier mobility, work function, hydrophilicity, and transparency can be adjusted by controlling the layer thickness or by surface treatment, and importantly, SB-free MSJs with dramatically lower contact resistance can be achieved. In this review, we systematically discussed the recent advances in 2D TMD-decorated MXene hybrid composites for electrochemical electrode-based applications such as batteries, supercapacitors, water splitting, and fuel cells. Among the 2D materials, MXenes and TMDs have advantages such as large specific area, good electrical properties, and an atomically thin layered structure, making them prominent candidates for various applications. In particular, the synergy from the construction of 2D heterojunctions between semiconducting TMDs and metallic MXenes could favorably influence electrochemical applications by modulating the work function or binding strength of the MSJ. Here, we present a comprehensive overview in Table 1, summarizing the synthesis approaches, material compositions, and applications of TMD-decorated MXenes as electrode materials for energy conversion and storage, which have been presented in recent years. In addition, recent developments have suggested the advantages of TMD-decorated MXene materials in diverse research applications.[84,108]

Because the electrocatalytic reaction takes place on the surface of the materials, research on MXenes with different termini on the basal plane, such as O, OH, or F, would be critical for such applications.[109] Therefore, careful surface modification of MXenes by controlling the amount and type of terminal elements will play a significant role in enhancing the performance of energy conversion applications using TMD–MXene hybrids. Furthermore, as described earlier, the surface termination of MXenes is affected by the type of etchant used for the extraction of the 'A' site atoms in MAX powders. Thus, MXenes with F-termini are often generated due to the frequent use of F-containing etchants such as HF. MXenes with different functional groups, such as F- and OH-terminated MXenes, may provide remarkable interactions with not only TMDs, but also reactants. Further diversification of the surface treatment is required to optimize or enhance the catalytic performance. For example, the metal-free sulfur nanoparticles could be treated on the surface of MXene by melt diffusion.[110] The strong interaction between Ti and S atoms can replace the hydroxyl groups on the MXene. To utilize the electronic interaction or hydrogen bonding formation, grafting charged or O-containing polymers, such as polyvinyl alcohol (PVA), poly(diallyldimethylammonium chloride (PDDA), poly(2-(dimethylamino)ethyl methacrylate (PDMAEMA), and sodium alginate (SA), onto MXene might be another great tool for surface engineering to modulate the

Table 1 Summary of synthesis, applications, and their performance of TMD/MXenes

| Parent materials | | | | Initial reversible capacity | Cycling performance | |
|---|---|---|---|---|---|---|
| TMD | MXene | Synthesis | | (mA h $g^{-1}$/A $g^{-1}$) | (residual capacity/cycles@$A^{-1}$) | Ref. |
| Li-ion batteries | | | | | | |
| $MoS_2$ | $Ti_3C_2$ | Hydrothermal | | 451.3/1 | 79%/1300@1 | 7*a* |
| $MoS_2$ | $V_4C_3$ | Hydrothermal | | 933.7/1 | 67%/450@1 | 76*a* |
| $MoS_2$ | $Ti_3C_2T_x$ | *In situ* sulfidation | | 554/0.1 | 92%/100@1 | 76*c* |
| $MoS_2$ | $Ti_3C_2T_x$ | Hydrothermal | | 339/0.1 | 98%/70@0.1 | 93 |
| $MoS_2$ | $Ti_3C_2$ | Solid state sintering | | 246.1/0.05 | 100%/200@0.1 | 72 |
| $MoS_2$ | $Ti_3C_2$ | Freeze-drying and thermal treatment | | 645.4/0.5 | 130%/1390@5 | 71*b* |
| $MoS_2$ | $Ti_3C_2$@C | Hydrothermal | | 1750/0.2 | 95%/3000@20 | 73 |
| $SnS_2/SnS_4$ | $Ti_3C_2T_x$ | Solvothermal and calcination | | 462.3/0.1 | 47%/500@5 | 11*e* |
| $MoS_2$ | $Ti_3C_2$ | Electrostatic attraction and (CTAB)-directed growth | | 914/0.1 | 100%/1000@0.5 | 75 |
| Na-ion batteries | | | | | | |
| $MoS_2$ | $Ti_3C_2$ | Electrostatic attraction and (CTAB)-directed growth | | 310/1 | — | 75 |
| $MoSe_2$ | $Ti_3C_2T_x$ | Hydrothermal | | 559/0.5 | 91%/400@2 | 57*a* |
| $SnS_2$ | $Ti_3C_2T_x$ | Hydrothermal | | 377/0.1 | 85%/200 @ 0.1 | 6 |
| $MoS_2$ | $Ti_3C_2T_x$ | Hydrothermal | | 285.4/0.1 | 88%/100 @ 0.1 | 11*g* |
| $MoS_2$ | $Ti_3C_2T_x$ | Hydrothermal | | 356.2/0.1 | 93%/70 @ 0.1 | 93 |
| Other batteries | | | | | | |
| $MoS_2$ | $Ti_3C_2T_x$ | Hydrothermal | K-ion | 233.1/0.1 | 75.9%/100@0.05 | 57*b* |
| $MoS_2$ | $Ti_3C_2T_x$ | Hydrothermal | Mg-ion | 165/0.5 | 65%/50@0.05 | 96*a* |
| 1T-2H $MoS_2$ | $Ti_3C_2$ | Hydrothermal | Li–S | 1014.1/0.5 C | 79%/300@0.5 C | 96*b* |

| TMD | MXene | synthesis | Specific capacitance | Ref. |
|---|---|---|---|---|
| Supercapacitor | | | | |
| $MoS_2$ | $Ti_3C_2T_x$ | Laser etching | 173.6 F $cm^{-3}$ | 58*e* |
| $1TWS_2$ | $Ti_3C_2$ | Sonication | 157 F $g^{-1}$ | 10 |

| TMD | MXene | Synthesis | Overpotential at 10 mA $cm^{-2}$ (mV) | Tafel slope (mV $dec^{-1}$) | Loading (mg $cm^{-2}$) | Electrolyte | Ref. |
|---|---|---|---|---|---|---|---|
| HER | | | | | | | |
| $MoS_2$ | $Mo_2CT_x$ | Hydrothermal | 176 | 98 | 0.71 | 1 M KOH | 76*b* |
| $MoS_2$ | $Ti_3C_2$ | Microwave heating | 110 | ~40 | 0.071 | 0.5 M $H_2SO_4$ | 74 |
| $MoS_2$ | $Ti_3C_2$@C | Hydrothermal | 135 | 45 | 0.4 | 0.5 M $H_2SO_4$ | 73 |
| $MoS_2$ | $Ti_3C_2$ | Hydrothermal | ~280 | 68 | — | 0.5 M $H_2SO_4$ | 105*a* |
| Co–$MoS_2$ | $Mo_2CT_x$ | Annealing | 112 | 82 | 0.354 | 1 M KOH | 105*b* |
| $MoSe_2$ | $Ti_3C_2$ | Hydrothermal | 180 | 91 | 0.28 | 0.5 M $H_2SO_4$ | 82 |
| 1T/2H $MoSe_2$ | $Ti_3C_2$ | Hydrothermal | 95 | 90 | 2~3 | 1 M KOH | 83 |
| OER | | | | | | | |
| $NbSe_2$ | $Nb_2C$ | Solid state sintering | 321 | 238 | ~2.65 | 1 M KOH | 107*b* |
| 1T/2H $MoSe_2$ | $Ti_3C_2$ | Hydrothermal | 340 | 91 | 2~3 | 1 M KOH | 83 |

| TMD | MXene | Synthesis | $E_{1/2}$ | Mass activity | Tafel slope (mV $dec^{-1}$) | Electrolyte | Ref. |
|---|---|---|---|---|---|---|---|
| ORR | | | | | | | |
| $MoS_2$ | $Ti_3C2Tx$ | Hydrothermal | 0.75 V | ~27 A $g^{-1}$ | 90 | 1 M KOH | 107*a* |

electrical and mechanical properties.[13,22c,111] However, surface engineering should address the persistent concern about restacking between the 2D materials due to van der Waals or hydrogen bonding interactions. Despite the efforts of many research groups, the facile oxidation of MXenes has not been fully resolved, leading to a deleterious impact on the catalytic performance of TMD/MXene composites. Thus, oxidative or oxygen-involved catalytic applications such as the OER or ORR would be negatively impacted by degradation problems. Catalyst architectures beyond the 2D–2D heterostructure should be considered, as specified in this review. The development of QD $MoS_2$ and MXenes on CNTs proved the possibility of other heterojunction types for electrochemical applications (ORR and MOR), although these species were deposited on the CNTs.[107a] Thus, improving and developing the interfacial and spatial design of TMD/MXene composites is inevitable for achieving advanced electrochemical applications.

Research on energy storage and conversion applications with TMD/MXene hybrids is in the infancy stage, and much has to be done to identify the ideal structural features, and synthesis routes. Thus far, complementary computational studies have been performed with various hypothetical TMD/MXene hybrid models, and many TMD/MXene hybrid candidates have been proposed as electrode materials for energy-related applications.

 

However, theoretical considerations are generally based on over-simplified and idealized models because of the limited computing resources, leading to an overly optimistic vision for these materials.[112] Therefore, it is necessary to develop methodologies for synthesizing structurally well-defined TMD/MXene hybrids, which are forecasted to afford excellent performance, and to test their performance. In doing so, the surface chemistry of TMD/MXene hybrids and their electrochemical reaction mechanisms should be probed carefully by both theoretical and experimental studies based on advanced *in situ* techniques, such as X-ray absorption spectroscopy (XAS), IR, Raman, and Mössbauer spectroscopy. Such studies would lead to the development of improved theoretical models that can fill the gap between experimentation and computation. Additionally, the emerging machine-learning technique would be beneficial for screening the possible composition, surface, and crystal structure of these materials for electrochemical applications, including the HER, OER, $CO_2$RR, and ORR. Finally, we hope that this review will accelerate investigations of the myriad combinations of TMD/MXene hybrids to realize the advent of next-generation energy-related technologies.

## Conflicts of interest

There are no conflicts to declare.

## Acknowledgements

This study was financially supported by the Department of Science and Technology (DST) under the joint India-Korea project (INT/Korea/P-52). This work was supported by the National Research Foundation of Korea (NRF-2020R1A2B5B03002475, NRF-2019R1A6A1A11044070, NRF-2019M3E6A1064709, NRF-2020R1A6A3A01096557, and NRF-2020K1A3A1A19088726), the Korea Basic Science Institute under the R&D program (Project No. C38530), Korea University Future Research Grant (KU-FRG), and Korea University Grant to T. K.

## References

1 (*a*) B.-M. Jun, S. Kim, J. Heo, C. M. Park, N. Her, M. Jang, Y. Huang, J. Han and Y. Yoon, Review of MXenes as new nanomaterials for energy storage/delivery and selected environmental applications, *Nano Res.*, 2019, **12**, 471–487; (*b*) F. Wang, X. Wu, X. Yuan, Z. Liu, Y. Zhang, L. Fu, Y. Zhu, Q. Zhou, Y. Wu and W. Huang, Latest advances in supercapacitors: from new electrode materials to novel device designs, *Chem. Soc. Rev.*, 2017, **46**, 6816–6854; (*c*) R. Yadav, A. Subhash, N. Chemmenchery and B. Kandasubramanian, Graphene and graphene oxide for fuel cell technology, *Ind. Eng. Chem. Res.*, 2018, **57**, 9333–9350.

2 (*a*) M. Armand and J.-M. Tarascon, Building better batteries, *Nature*, 2008, **451**, 652–657; (*b*) P. Simon and Y. Gogotsi, Materials for electrochemical capacitors, *Nat. Mater.*, 2008, **7**, 845–854; (*c*) M. R. Lukatskaya, B. Dunn and Y. Gogotsi, Multidimensional materials and device architectures for future hybrid energy storage, *Nat. Commun.*, 2016, **7**, 12647; (*d*) Q. Pang, X. Liang, C. Y. Kwok and L. F. Nazar, Advances in lithium–sulfur batteries based on multifunctional cathodes and electrolytes, *Nat. Energy*, 2016, **1**, 16132; (*e*) Y. Zheng and S.-Z. Qiao, N-doping goes *sp*-hybridized, *Nat. Chem.*, 2018, **10**, 900–902; (*f*) Y. Zhao, N. Yang, H. Yao, D. Liu, L. Song, J. Zhu, S. Li, L. Gu, K. Lin and D. Wang, Stereodefined Codoping of sp-N and S Atoms in Few-Layer Graphdiyne for Oxygen Evolution Reaction, *J. Am. Chem. Soc.*, 2019, **141**, 7240–7244.

3 C. Tan, X. Cao, X.-J. Wu, Q. He, J. Yang, X. Zhang, J. Chen, W. Zhao, S. Han, G.-H. Nam, M. Sindoro and H. Zhang, Recent advances in ultrathin two-dimensional nanomaterials, *Chem. Rev.*, 2017, **117**, 6225–6331.

4 (*a*) Y. Sun, D. Chen and Z. Liang, Two-dimensional MXenes for energy storage and conversion applications, *Mater. Today, Energy*, 2017, **5**, 22–36; (*b*) M.-Q. Zhao, M. Torelli, C. E. Ren, M. Ghidiu, Z. Ling, B. Anasori, M. W. Barsoum and Y. Gogotsi, 2D titanium carbide and transition metal oxides hybrid electrodes for Li-ion storage, *Nano Energy*, 2016, **30**, 603–613; (*c*) B. Anasori, M. R. Lukatskaya and Y. Gogotsi, 2D metal carbides and nitrides (MXenes) for energy storage, *Nat. Rev. Mater.*, 2017, **2**, 16098.

5 D. Xiong, X. Li, Z. Bai and S. Lu, Recent advances in layered $Ti_3C_2T_x$ MXene for electrochemical energy storage, *Small*, 2018, **14**, 1703419.

6 Y. Wu, P. Nie, L. Wu, H. Dou and X. Zhang, 2D MXene/$SnS_2$ composites as high-performance anodes for sodium ion batteries, *Chem. Eng. J.*, 2018, **334**, 932–938.

7 (*a*) S. Luan, M. Han, Y. Xi, K. Wei, Y. Wang, J. Zhou, L. Hou and F. Gao, $MoS_2$-decorated 2D $Ti_3C_2$ (MXene): a high-performance anode material for lithium-ion batteries, *Ionics*, 2020, **26**, 51–59; (*b*) M. Q. Zhao, X. Xie, C. E. Ren, T. Makaryan, B. Anasori, G. Wang and Y. Gogotsi, Hollow MXene spheres and 3D macroporous MXene frameworks for Na-ion storage, *Adv. Mater.*, 2017, **29**, 1702410.

8 (*a*) W. Choi, N. Choudhary, G. H. Han, J. Park, D. Akinwande and Y. H. Lee, Recent development of two-dimensional transition metal dichalcogenides and their applications, *Mater. Today*, 2017, **20**, 116–130; (*b*) S. Manzeli, D. Ovchinnikov, D. Pasquier, O. V. Yazyev and A. Kis, 2D transition metal dichalcogenides, *Nat. Rev. Mater.*, 2017, **2**, 17033.

9 (*a*) M. Chhowalla, H. S. Shin, G. Eda, L.-J. Li, K. P. Loh and H. Zhang, The chemistry of two-dimensional layered transition metal dichalcogenide nanosheets, *Nat. Chem.*, 2013, **5**, 263–275; (*b*) L. Lin, P. Sherrell, Y. Liu, W. Lei, S. Zhang, H. Zhang, G. G. Wallace and J. Chen, Engineered 2D Transition Metal Dichalcogenides—A Vision of Viable Hydrogen Evolution Reaction Catalysis, *Adv. Energy Mater.*, 2020, **10**, 1903870.

10 J. Vyskočil, C. C. Mayorga-Martinez, K. Szőkölová, A. Dash, J. Gonzalez-Julian, Z. Sofer and M. Pumera, 2D Stacks of MXene $Ti_3C_2$ and 1T-Phase $WS_2$ with Enhanced Capacitive Behavior, *ChemElectroChem*, 2019, **6**, 3982–3986.

11 (*a*) J. You, C. Si, J. Zhou and Z. Sun, Contacting $MoS_2$ to MXene: Vanishing p-Type Schottky Barrier and Enhanced Hydrogen Evolution Catalysis, *J. Phys. Chem. C*, 2019, **123**, 3719–3726; (*b*) Y. Shao, Q. Wang, H. Pan and X. Shi,

van der Waals Contact to 2D Semiconductors with a Switchable Electric Dipole: Achieving Both n- and p-Type Ohmic Contacts to Metals with a Wide Range of Work Functions, *Adv. Electron. Mater.*, 2020, **6**, 1900981; (*c*) J. Wang, X. Zhou, M. Yang, D. Cao, X. Chen and H. Shu, Interface and polarization effects induced Schottky-barrier-free contacts in two-dimensional MXene/GaN heterojunctions, *J. Mater. Chem. C*, 2020, **8**, 7350–7357; (*d*) Q. Wang, K. Dou and X. Shi, Band alignment in multilayered semiconductor homojunctions supported on metals, *J. Mater. Chem. C*, 2020, **8**, 959–967; (*e*) J. Li, L. Han, Y. Li, J. Li, G. Zhu, X. Zhang, T. Lu and L. Pan, MXene-decorated $SnS_2/Sn_3S_4$ hybrid as anode material for high-rate lithium-ion batteries, *Chem. Eng. J.*, 2020, **380**, 122590; (*f*) M. Chen, Z. Zheng, Q. Wang, Y. Zhang, X. Ma, C. Shen, D. Xu, J. Liu, Y. Liu, P. Gionet, I. O'Connor, L. Pinnell, J. Wang, E. Gratz, R. Arsenault and Y. Wang, Closed Loop Recycling of Electric Vehicle Batteries to Enable Ultra-high Quality Cathode Powder, *Sci. Rep.*, 2019, **9**, 1654; (*g*) Y. Wu, P. Nie, J. Jiang, B. Ding, H. Dou and X. Zhang, $MoS_2$-Nanosheet-Decorated 2D Titanium Carbide (MXene) as High-Performance Anodes for Sodium-Ion Batteries, *ChemElectroChem*, 2017, **4**, 1560–1565.

12 (*a*) V. M. H. Ng, H. Huang, K. Zhou, P. S. Lee, W. Que, J. Z. Xu and L. B. Kong, Recent progress in layered transition metal carbides and/or nitrides (MXenes) and their composites: synthesis and applications, *J. Mater. Chem. A*, 2017, **5**, 3039–3068; (*b*) X. Chia, A. Y. S. Eng, A. Ambrosi, S. M. Tan and M. Pumera, Electrochemistry of nanostructured layered transition-metal dichalcogenides, *Chem. Rev.*, 2015, **115**, 11941–11966; (*c*) N. Hemanth and B. Kandasubramanian, Recent advances in 2D MXenes for enhanced cation intercalation in energy harvesting applications: a review, *Chem. Eng. J.*, 2020, **392**, 123678.

13 F. Shahzad, M. Alhabeb, C. B. Hatter, B. Anasori, S. M. Hong, C. M. Koo and Y. Gogotsi, Electromagnetic interference shielding with 2D transition metal carbides (MXenes), *Science*, 2016, **353**, 1137–1140.

14 (*a*) C. Eames and M. S. Islam, Ion intercalation into two-dimensional transition-metal carbides: global screening for new high-capacity battery materials, *J. Am. Chem. Soc.*, 2014, **136**, 16270–16276; (*b*) M. R. Lukatskaya, S. Kota, Z. Lin, M.-Q. Zhao, N. Shpigel, M. D. Levi, J. Halim, P.-L. Taberna, M. W. Barsoum, P. Simon and Y. Gogotsi, Ultra-high-rate pseudocapacitive energy storage in two-dimensional transition metal carbides, *Nat. Energy*, 2017, **2**, 17105.

15 M. Ghidiu, M. R. Lukatskaya, M.-Q. Zhao, Y. Gogotsi and M. W. Barsoum, Conductive two-dimensional titanium carbide 'clay'with high volumetric capacitance, *Nature*, 2014, **516**, 78–81.

16 M. R. Lukatskaya, O. Mashtalir, C. E. Ren, Y. Dall'Agnese, P. Rozier, P. L. Taberna, M. Naguib, P. Simon, M. W. Barsoum and Y. Gogotsi, Cation intercalation and high volumetric capacitance of two-dimensional titanium carbide, *Science*, 2013, **341**, 1502–1505.

17 X. Wang, C. Garnero, G. Rochard, D. Magne, S. Morisset, S. Hurand, P. Chartier, J. Rousseau, T. Cabioc'h, C. Coutanceau, V. Mauchamp and S. Célérier, A new etching environment ($FeF_3$/HCl) for the synthesis of two-dimensional titanium carbide MXenes: a route towards selective reactivity *vs.* water, *J. Mater. Chem. A*, 2017, **5**, 22012–22023.

18 P. Urbankowski, B. Anasori, T. Makaryan, D. Er, S. Kota, P. L. Walsh, M. Zhao, V. B. Shenoy, M. W. Barsoum and Y. Gogotsi, Synthesis of two-dimensional titanium nitride $Ti_4N_3$ (MXene), *Nanoscale*, 2016, **8**, 11385–11391.

19 C. Xu, L. Wang, Z. Liu, L. Chen, J. Guo, N. Kang, X.-L. Ma, H.-M. Cheng and W. Ren, Large-area high-quality 2D ultrathin $Mo_2C$ superconducting crystals, *Nat. Mater.*, 2015, **14**, 1135–1141.

20 L. Verger, C. Xu, V. Natu, H.-M. Cheng, W. Ren and M. W. Barsoum, Overview of the synthesis of MXenes and other ultrathin 2D transition metal carbides and nitrides, *Curr. Opin. Solid State Mater. Sci.*, 2019, **23**, 149–163.

21 (*a*) J. Halim, S. Kota, M. R. Lukatskaya, M. Naguib, M. Q. Zhao, E. J. Moon, J. Pitock, J. Nanda, S. J. May, Y. Gogotsi and M. W. Barsoum, Synthesis and characterization of 2D molybdenum carbide (MXene), *Adv. Funct. Mater.*, 2016, **26**, 3118–3127; (*b*) J. Zhou, X. Zha, F. Y. Chen, Q. Ye, P. Eklund, S. Du and Q. Huang, A two-dimensional zirconium carbide by selective etching of $Al_3C_3$ from nanolaminated $Zr_3Al_3C_5$, *Angew. Chem., Int. Ed.*, 2016, **55**, 5008–5013.

22 (*a*) O. Mashtalir, M. Naguib, V. N. Mochalin, Y. Dall'Agnese, M. Heon, M. W. Barsoum and Y. Gogotsi, Intercalation and delamination of layered carbides and carbonitrides, *Nat. Commun.*, 2013, **4**, 1716; (*b*) M. Naguib, R. R. Unocic, B. L. Armstrong and J. Nanda, Large-scale delamination of multi-layers transition metal carbides and carbonitrides ''MXenes'', *Dalton Trans.*, 2015, **44**, 9353–9358; (*c*) Z. Ling, C. E. Ren, M.-Q. Zhao, J. Yang, J. M. Giammarco, J. Qiu, M. W. Barsoum and Y. Gogotsi, Flexible and conductive MXene films and nanocomposites with high capacitance, *Proc. Natl. Acad. Sci. U. S. A.*, 2014, **111**, 16676–16681.

23 T. Hu, M. Hu, Z. Li, H. Zhang, C. Zhang, J. Wang and X. Wang, Interlayer coupling in two-dimensional titanium carbide MXenes, *Phys. Chem. Chem. Phys.*, 2016, **18**, 20256–20260.

24 (*a*) J. Pang, R. G. Mendes, A. Bachmatiuk, L. Zhao, H. Q. Ta, T. Gemming, H. Liu, Z. Liu and M. H. Rummeli, Applications of 2D MXenes in energy conversion and storage systems, *Chem. Soc. Rev.*, 2019, **48**, 72–133; (*b*) A. L. Ivanovskii and A. N. Enyashin, Graphene-like transition-metal nanocarbides and nanonitrides, *Russ. Chem. Rev.*, 2013, **82**, 735–746.

25 (*a*) H. Kim, Z. Wang and H. N. Alshareef, MXetronics: Electronic and photonic applications of MXenes, *Nano Energy*, 2019, **60**, 179–197; (*b*) L. Chen, X. Shi, N. Yu, X. Zhang, X. Du and J. Lin, Measurement and analysis of thermal conductivity of $Ti_3C_2T_x$ MXene films, *Materials*, 2018, **11**, 1701; (*c*) Z. Fu, N. Wang, D. Legut, C. Si, Q. Zhang, S. Du, T. C. Germann, J. S. Francisco and R. Zhang, Rational design of flexible two-dimensional MXenes with multiple functionalities, *Chem. Rev.*, 2019,

 

**119**, 11980–12031; (*d*) X.-H. Zha, Q. Huang, J. He, H. He, J. Zhai, J. S. Francisco and S. Du, The thermal and electrical properties of the promising semiconductor MXene $Hf_2CO_2$, *Sci. Rep.*, 2016, **6**, 27971.

26 T. Hu, J. Yang, W. Li, X. Wang and C. M. Li, Quantifying the rigidity of 2D carbides (MXenes), *Phys. Chem. Chem. Phys.*, 2020, **22**, 2115–2121.

27 L. Verger, V. Natu, M. Carey and M. W. Barsoum, MXenes: an introduction of their synthesis, select properties, and applications, *Trends Chem.*, 2019, **1**, 656–669.

28 M. Khazaei, A. Ranjbar, M. Arai, T. Sasaki and S. Yunoki, Electronic properties and applications of MXenes: a theoretical review, *J. Mater. Chem. C*, 2017, **5**, 2488–2503.

29 R. M. Ronchi, J. T. Arantes and S. F. Santos, Synthesis, structure, properties and applications of MXenes: Current status and perspectives, *Ceram. Int.*, 2019, **45**, 18167–18188.

30 Y. Xie and P. R. C. Kent, Hybrid density functional study of structural and electronic properties of functionalized $Ti_{n+1}X_n$ (X = C, N) monolayers, *Phys. Rev. B: Condens. Matter Mater. Phys.*, 2013, **87**, 235441.

31 (*a*) K. Rasool, R. P. Pandey, P. A. Rasheed, S. Buczek, Y. Gogotsi and K. A. Mahmoud, Water treatment and environmental remediation applications of two-dimensional metal carbides (MXenes), *Mater. Today*, 2019, **30**, 80–102; (*b*) J. Zhu, E. Ha, G. Zhao, Y. Zhou, D. Huang, G. Yue, L. Hu, N. Sun, Y. Wang, L. Y. S. Lee, C. Xu, K.-Y. Wong, D. Astruc and P. Zhao, Recent advance in MXenes: A promising 2D material for catalysis, sensor and chemical adsorption, *Coord. Chem. Rev.*, 2017, **352**, 306–327; (*c*) K. Huang, Z. Li, J. Lin, G. Han and P. Huang, Two-dimensional transition metal carbides and nitrides (MXenes) for biomedical applications, *Chem. Soc. Rev.*, 2018, **47**, 5109–5124.

32 (*a*) M. Greaves, S. Barg and M. A. Bissett, MXene-Based Anodes for Metal-Ion Batteries, *Batteries Supercaps*, 2020, **3**, 214–235; (*b*) V. Bayram, M. Ghidiu, J. J. Byun, S. D. Rawson, P. Yang, S. A. McDonald, M. Lindley, S. Fairclough, S. J. Haigh, P. J. Withers, M. W. Barsoum, I. A. Kinloch and S. Barg, MXene Tunable Lamellae Architectures for Supercapacitor Electrodes, *ACS Appl. Energy Mater.*, 2020, **3**, 411–422; (*c*) G. Gao, A. P. O'Mullane and A. Du, 2D MXenes: a new family of promising catalysts for the hydrogen evolution reaction, *ACS Catal.*, 2017, **7**, 494–500; (*d*) T. P. Nguyen, D. M. T. Nguyen, H. K. Le, D.-V. N. Vo, S. S. Lam, R. S. Varma, M. Shokouhimehr, C. C. Nguyen and Q. Van, Le, MXenes: Applications in electrocatalytic, photocatalytic hydrogen evolution reaction and $CO_2$ reduction, *Mol. Catal.*, 2020, **486**, 110850; (*e*) R. Zang, P. Li and G. Wang, Bimetallic Sulfide/Sulfur Doped $T_3C_2T_x$ MXene Nanocomposites as High-performance Anode Materials for Sodium-ion Batteries, *Chem. Res. Chin. Univ.*, 2020, **36**, 431–438.

33 J. Nan, X. Guo, J. Xiao, X. Li, W. Chen, W. Wu, H. Liu, Y. Wang, M. Wu and G. Wang, Nanoengineering of 2D MXene-based materials for energy storage applications, *Small*, 2019, 1902085.

34 H. Li, J. Wu, Z. Yin and H. Zhang, Preparation and applications of mechanically exfoliated single-layer and multilayer $MoS_2$ and $WSe_2$ nanosheets, *Acc. Chem. Res.*, 2014, **47**, 1067–1075.

35 (*a*) M. Ahmadi, O. Zabihi, S. Jeon, M. Yoonessi, A. Dasari, S. Ramakrishna and M. Naebe, 2D transition metal dichalcogenide nanomaterials: advances, opportunities, and challenges in multi-functional polymer nanocomposites, *J. Mater. Chem. A*, 2020, **8**, 845–883; (*b*) G. Eda, H. Yamaguchi, D. Voiry, T. Fujita, M. Chen and M. Chhowalla, Photoluminescence from chemically exfoliated $MoS_2$, *Nano Lett.*, 2011, **11**, 5111–5116.

36 B. Adilbekova, Y. Lin, E. Yengel, H. Faber, G. Harrison, Y. Firdaus, A. El-Labban, D. H. Anjum, V. Tung and T. D. Anthopoulos, Liquid phase exfoliation of $MoS_2$ and $WS_2$ in aqueous ammonia and their application in highly efficient organic solar cells, *J. Mater. Chem. C*, 2020, **8**, 5259–5264.

37 (*a*) B. A. Joyce, Molecular beam epitaxy, *Rep. Prog. Phys.*, 1985, **48**, 1637–1697; (*b*) W. Pacuski, M. Grzeszczyk, K. Nogajewski, A. Bogucki, K. Oreszczuk, J. Kucharek, K. E. Połczyńska, B. Seredyński, A. Rodek, R. Bożek, T. Taniguchi, K. Watanabe, S. Kret, J. Sadowski, T. Kazimierczuk, M. Potemski and P. Kossacki, Narrow Excitonic Lines and Large-Scale Homogeneity of Transition-Metal Dichalcogenide Monolayers Grown by Molecular Beam Epitaxy on Hexagonal Boron Nitride, *Nano Lett.*, 2020, **20**, 3058–3066.

38 (*a*) C. Cong, J. Shang, X. Wu, B. Cao, N. Peimyoo, C. Qiu, L. Sun and T. Yu, Synthesis and Optical Properties of Large-Area Single-Crystalline 2D Semiconductor $WS_2$ Monolayer from Chemical Vapor Deposition, *Adv. Opt. Mater.*, 2014, **2**, 131–136; (*b*) Y. H. Lee, X. Q. Zhang, W. Zhang, M. T. Chang, C. T. Lin, K. D. Chang, Y. C. Yu, J. T. W. Wang, C. S. Chang, L. J. Li and T.-W. Lin, Synthesis of large-area $MoS_2$ atomic layers with chemical vapor deposition, *Adv. Mater.*, 2012, **24**, 2320–2325; (*c*) S. Najmaei, Z. Liu, W. Zhou, X. Zou, G. Shi, S. Lei, B. I. Yakobson, J.-C. Idrobo, P. M. Ajayan and J. Lou, Vapour phase growth and grain boundary structure of molybdenum disulphide atomic layers, *Nat. Mater.*, 2013, **12**, 754–759; (*d*) T. A. Empante, Y. Zhou, V. Klee, A. E. Nguyen, I. H. Lu, M. D. Valentin, S. A. Naghibi Alvillar, E. Preciado, A. J. Berges, C. S. Merida, M. Gomez, S. Bobek, M. Isarraraz, E. J. Reed and L. Bartels, Chemical Vapor Deposition Growth of Few-Layer $MoTe_2$ in the 2H, 1T′, and 1T Phases: Tunable Properties of $MoTe_2$ Films, *ACS Nano*, 2017, **11**, 900–905; (*e*) X. Wang, Y. Gong, G. Shi, W. L. Chow, K. Keyshar, G. Ye, R. Vajtai, J. Lou, Z. Liu, E. Ringe, B. K. Tay and P. M. Ajayan, Chemical Vapor Deposition Growth of Crystalline Monolayer $MoSe_2$, *ACS Nano*, 2014, **8**, 5125–5131.

39 (*a*) Y.-F. Lim, K. Priyadarshi, F. Bussolotti, P. K. Gogoi, X. Cui, M. Yang, J. Pan, S. W. Tong, S. Wang, S. J. Pennycook, K. E. J. Goh, A. T. S. Wee, S. L. Wong and D. Chi, Modification of Vapor Phase Concentrations in $MoS_2$ Growth Using a NiO Foam Barrier, *ACS Nano*, 2018, **12**, 1339–1349; (*b*) D. Li, Z. Xiao, S. Mu, F. Wang, Y. Liu,

J. Song, X. Huang, L. Jiang, J. Xiao, L. Liu, S. Ducharme, B. Cui, X. Hong, L. Jiang, J.-F. Silvain and Y. Lu, A Facile Space-Confined Solid-Phase Sulfurization Strategy for Growth of High-Quality Ultrathin Molybdenum Disulfide Single Crystals, *Nano Lett.*, 2018, **18**, 2021–2032; (*c*) Y. Zhang, Q. Ji, G.-F. Han, J. Ju, J. Shi, D. Ma, J. Sun, Y. Zhang, M. Li, X.-Y. Lang, Y. Zhang and Z. Liu, Dendritic, Transferable, Strictly Monolayer $MoS_2$ Flakes Synthesized on $SrTiO_3$ Single Crystals for Efficient Electrocatalytic Applications, *ACS Nano*, 2014, **8**, 8617–8624; (*d*) D. Wu, T. Min, J. Zhou, C. Li, G. Ma, G. Lu, M. Xia and Z. Gu, Effect of Substrate symmetry on the dendrite morphology of $MoS_2$ Film synthesized by CVD, *Sci. Rep.*, 2017, **7**, 15166.

40 G. W. Shim, W. Hong, S. Y. Yang and S.-Y. Choi, Tuning the catalytic functionality of transition metal dichalcogenides grown by chemical vapour deposition, *J. Mater. Chem. A*, 2017, **5**, 14950–14968.

41 (*a*) Y. Zhan, Z. Liu, S. Najmaei, P. M. Ajayan and J. Lou, Large-Area Vapor-Phase Growth and Characterization of $MoS_2$ Atomic Layers on a $SiO_2$ Substrate, *Small*, 2012, **8**, 966–971; (*b*) J. Park, N. Choudhary, J. Smith, G. Lee, M. Kim and W. Choi, Thickness modulated $MoS_2$ grown by chemical vapor deposition for transparent and flexible electronic devices, *Appl. Phys. Lett.*, 2015, **106**, 012104.

42 (*a*) K.-K. Liu, W. Zhang, Y.-H. Lee, Y.-C. Lin, M.-T. Chang, C.-Y. Su, C.-S. Chang, H. Li, Y. Shi, H. Zhang, C.-S. Lai and L.-J. Li, Growth of large-area and highly crystalline $MoS_2$ thin layers on insulating substrates, *Nano Lett.*, 2012, **12**, 1538–1544; (*b*) A. Hasani, Q. V. Le, M. Tekalgne, M.-J. Choi, S. Choi, T. H. Lee, H. Kim, S. H. Ahn, H. W. Jang and S. Y. Kim, Fabrication of a WS2/p-Si Heterostructure Photocathode Using Direct Hybrid Thermolysis, *ACS Appl. Mater. Interfaces*, 2019, **11**, 29910–29916.

43 (*a*) K. Kang, S. Xie, L. Huang, Y. Han, P. Y. Huang, K. F. Mak, C.-J. Kim, D. Muller and J. Park, High-mobility three-atom-thick semiconducting films with wafer-scale homogeneity, *Nature*, 2015, **520**, 656–660; (*b*) S. M. Eichfeld, L. Hossain, Y.-C. Lin, A. F. Piasecki, B. Kupp, A. G. Birdwell, R. A. Burke, N. Lu, X. Peng, J. Li, A. Azcatl, S. McDonnell, R. M. Wallace, M. J. Kim, T. S. Mayer, J. M. Redwing and J. A. Robinson, Highly scalable, atomically thin $WSe_2$ grown via metal–organic chemical vapor deposition, *ACS Nano*, 2015, **9**, 2080–2087; (*c*) B. Kalanyan, W. A. Kimes, R. Beams, S. J. Stranick, E. Garratt, I. Kalish, A. V. Davydov, R. K. Kanjolia and J. E. Maslar, Rapid wafer-scale growth of polycrystalline 2H-$MoS_2$ by pulsed metal–organic chemical vapor deposition, *Chem. Mater.*, 2017, **29**, 6279–6288.

44 A. Cohen, A. Patsha, P. K. Mohapatra, M. Kazes, K. Ranganathan, L. Houben, D. Oron and A. Ismach, Growth-Etch Metal–Organic Chemical Vapor Deposition Approach of $WS_2$ Atomic Layers, *ACS Nano*, 2021, **15**, 526–538.

45 (*a*) L. K. Tan, B. Liu, J. H. Teng, S. Guo, H. Y. Low and K. P. Loh, Atomic layer deposition of a $MoS_2$ film, *Nanoscale*, 2014, **6**, 10584–10588; (*b*) J.-G. Song, J. Park, W. Lee, T. Choi, H. Jung, C. W. Lee, S.-H. Hwang, J. M. Myoung, J.-H. Jung, S.-H. Kim, C. Lansalot-Matras and H. Kim, Layer-controlled, wafer-scale, and conformal synthesis of tungsten disulfide nanosheets using atomic layer deposition, *ACS Nano*, 2013, **7**, 11333–11340; (*c*) G.-H. Park, K. Nielsch and A. Thomas, 2D Transition Metal Dichalcogenide Thin Films Obtained by Chemical Gas Phase Deposition Techniques, *Adv. Mater. Interfaces*, 2019, **6**, 1800688.

46 (*a*) S. Balasubramanyam, M. J. M. Merkx, M. A. Verheijen, W. M. M. Kessels, A. J. M. Mackus and A. A. Bol, Area-Selective Atomic Layer Deposition of Two-Dimensional $WS_2$ Nanolayers, *ACS Mater. Lett.*, 2020, **2**, 511–518; (*b*) C. Yue, Y. Wang, H. Liu, L. Chen, H. Zhu and Q. Sun, Controlled growth of $MoS_2$ by atomic layer deposition on patterned gold pads, *J. Cryst. Growth*, 2020, **541**, 125683.

47 J. A. Wilson and A. Yoffe, The transition metal dichalcogenides discussion and interpretation of the observed optical, electrical and structural properties, *Adv. Phys.*, 1969, **18**, 193–335.

48 R. Lv, J. A. Robinson, R. E. Schaak, D. Sun, Y. Sun, T. E. Mallouk and M. Terrones, Transition metal dichalcogenides and beyond: synthesis, properties, and applications of single-and few-layer nanosheets, *Acc. Chem. Res.*, 2015, **48**, 56–64.

49 S. Bertolazzi, J. Brivio and A. Kis, Stretching and breaking of ultrathin $MoS_2$, *ACS Nano*, 2011, **5**, 9703–9709.

50 K. F. Mak, C. Lee, J. Hone, J. Shan and T. F. Heinz, Atomically thin $MoS_2$: a new direct-gap semiconductor, *Phys. Rev. Lett.*, 2010, **105**, 136805.

51 (*a*) B. Radisavljevic, A. Radenovic, J. Brivio, V. Giacometti and A. Kis, Single-layer $MoS_2$ transistors, *Nat. Nanotechnol.*, 2011, **6**, 147–150; (*b*) Q. H. Wang, K. Kalantar-Zadeh, A. Kis, J. N. Coleman and M. S. Strano, Electronics and optoelectronics of two-dimensional transition metal dichalcogenides, *Nat. Nanotechnol.*, 2012, **7**, 699–712.

52 M. Pumera, Z. Sofer and A. Ambrosi, Layered transition metal dichalcogenides for electrochemical energy generation and storage, *J. Mater. Chem. A*, 2014, **2**, 8981–8987.

53 (*a*) H. Li, Z. Yin, Q. He, H. Li, X. Huang, G. Lu, D. W. H. Fam, A. I. Y. Tok, Q. Zhang and H. Zhang, Fabrication of Single- and Multilayer $MoS_2$ Film-Based Field-Effect Transistors for Sensing NO at Room Temperature, *Small*, 2012, **8**, 63–67; (*b*) J. Ping, Z. Fan, M. Sindoro, Y. Ying and H. Zhang, Recent advances in sensing applications of two-dimensional transition metal dichalcogenide nanosheets and their composites, *Adv. Funct. Mater.*, 2017, **27**, 1605817.

54 (*a*) U. Gupta and C. N. R. Rao, Hydrogen generation by water splitting using $MoS_2$ and other transition metal dichalcogenides, *Nano Energy*, 2017, **41**, 49–65; (*b*) D. Voiry, H. Yamaguchi, J. Li, R. Silva, D. C. Alves, T. Fujita, M. Chen, T. Asefa, V. B. Shenoy, G. Eda and M. Chhowalla, Enhanced catalytic activity in strained chemically exfoliated $WS_2$ nanosheets for hydrogen evolution, *Nat. Mater.*, 2013, **12**, 850–855; (*c*) M. A. Lukowski, A. S. Daniel, F. Meng, A. Forticaux, L. Li and S. Jin, Enhanced hydrogen evolution catalysis from chemically exfoliated metallic $MoS_2$ nanosheets, *J. Am. Chem. Soc.*, 2013, **135**, 10274–10277.

 

55 (*a*) K. F. Mak and J. Shan, Photonics and optoelectronics of 2D semiconductor transition metal dichalcogenides, *Nat. Photonics*, 2016, **10**, 216–226; (*b*) H. Wang, L. Yu, Y.-H. Lee, Y. Shi, A. Hsu, M. L. Chin, L.-J. Li, M. Dubey, J. Kong and T. Palacios, Integrated Circuits Based on Bilayer $MoS_2$ Transistors, *Nano Lett.*, 2012, **12**, 4674–4680.

56 (*a*) M. Acerce, D. Voiry and M. Chhowalla, Metallic 1T phase $MoS_2$ nanosheets as supercapacitor electrode materials, *Nat. Nanotechnol.*, 2015, **10**, 313–318; (*b*) X. Xie, Z. Ao, D. Su, J. Zhang and G. Wang, $MoS_2$/Graphene Composite Anodes with Enhanced Performance for Sodium-Ion Batteries: The Role of the Two-Dimensional Heterointerface, *Adv. Funct. Mater.*, 2015, **25**, 1393–1403; (*c*) K. Chang and W. Chen, In situ synthesis of $MoS_2$/graphene nanosheet composites with extraordinarily high electrochemical performance for lithium ion batteries, *Chem. Commun.*, 2011, **47**, 4252–4254; (*d*) N. Choudhary, M. Patel, Y.-H. Ho, N. B. Dahotre, W. Lee, J. Y. Hwang and W. Choi, Directly deposited $MoS_2$ thin film electrodes for high performance supercapacitors, *J. Mater. Chem. A*, 2015, **3**, 24049–24054.

57 (*a*) E. Xu, Y. Zhang, H. Wang, Z. Zhu, J. Quan, Y. Chang, P. Li, D. Yu and Y. Jiang, Ultrafast kinetics net electrode assembled via $MoSe_2$/MXene heterojunction for high-performance sodium-ion batteries, *Chem. Eng. J.*, 2020, **385**, 123839; (*b*) J. Li, B. Rui, W. Wei, P. Nie, L. Chang, Z. Le, M. Liu, H. Wang, L. Wang and X. Zhang, Nanosheets assembled layered $MoS_2$/MXene as high performance anode materials for potassium ion batteries, *J. Power Sources*, 2020, **449**, 227481.

58 (*a*) J. Liu, Y. Liu, D. Xu, Y. Zhu, W. Peng, Y. Li, F. Zhang and X. Fan, Hierarchical ''nanoroll'' like $MoS_2/Ti_3C_2T_x$ hybrid with high electrocatalytic hydrogen evolution activity, *Appl. Catal., B*, 2019, **241**, 89–94; (*b*) Y. Li, S. Yang, Z. Liang, Y. Xue, H. Cui and J. Tian, 1T-$MoS_2$ nanopatch/$Ti_3C_2$ MXene/$TiO_2$ nanosheet hybrids for efficient photocatalytic hydrogen evolution, *Mater. Chem. Front.*, 2019, **3**, 2673–2680; (*c*) W. Jiang, X. Zou, H. Du, L. Gan, C. Xu, F. Kang, W. Duan and J. Li, Universal descriptor for large-scale screening of high-performance mxene-based materials for energy storage and conversion, *Chem. Mater.*, 2018, **30**, 2687–2693; (*d*) Y. Li, L. Ding, Z. Liang, Y. Xue, H. Cui and J. Tian, Synergetic effect of defects rich $MoS_2$ and $Ti_3C_2$ MXene as cocatalysts for enhanced photocatalytic $H_2$ production activity of $TiO_2$, *Chem. Eng. J.*, 2020, **383**, 123178; (*e*) X. Chen, S. Wang, J. Shi, X. Du, Q. Cheng, R. Xue, Q. Wang, M. Wang, L. Ruan and W. Zeng, Direct Laser Etching Free-Standing MXene-$MoS_2$ Film for Highly Flexible Micro-Supercapacitor, *Adv. Mater. Interfaces*, 2019, **6**, 1901160.

59 (*a*) N. F. Mott, The theory of crystal rectifiers, *Proc. R. Soc. London, Ser. A*, 1939, **171**, 27–38; (*b*) W. Schottky, Zur halbleitertheorie der sperrschicht-und spitzengleichrichter, *Z. Phys.*, 1939, **113**, 367–414.

60 Y. Liu, H. Xiao and W. A. Goddard, Schottky–Barrier-Free Contacts with Two-Dimensional Semiconductors by Surface-Engineered MXenes, *J. Am. Chem. Soc.*, 2016, **138**, 15853–15856.

61 (*a*) S. M. Sze and K. K. Ng, *Physics of semiconductor devices*, John Wiley & Sons, Inc., Hoboken, NJ, USA, 2006; (*b*) P. Schmid, Silicide-silicon Schottky barriers, *Helv. Phys. Acta*, 1985, **58**, 371–382; (*c*) W. Mönch, On metal-semiconductor surface barriers, *Surf. Sci.*, 1970, **21**, 443–446; (*d*) J. R. Waldrop, Schottky-barrier height of ideal metal contacts to GaAs, *Appl. Phys. Lett.*, 1984, **44**, 1002–1004; (*e*) A. Cowley and S. Sze, Surface states and barrier height of metal-semiconductor systems, *J. Appl. Phys.*, 1965, **36**, 3212–3220.

62 R. T. Tung, The physics and chemistry of the Schottky barrier height, *Appl. Phys. Rev.*, 2014, **1**, 011304.

63 A. Franciosi and C. G. Van de Walle, Heterojunction band offset engineering, *Surf. Sci. Rep.*, 1996, **25**, 1–140.

64 (*a*) Y. Liu, J. Guo, E. Zhu, L. Liao, S.-J. Lee, M. Ding, I. Shakir, V. Gambin, Y. Huang and X. Duan, Approaching the Schottky–Mott limit in van der Waals metal–semiconductor junctions, *Nature*, 2018, **557**, 696–700; (*b*) Y. Liu, P. Stradins and S.-H. Wei, van der Waals metal-semiconductor junction: Weak Fermi level pinning enables effective tuning of Schottky barrier, *Sci. Adv.*, 2016, **2**, e1600069.

65 (*a*) S. Das, H.-Y. Chen, A. V. Penumatcha and J. Appenzeller, High performance multilayer $MoS_2$ transistors with scandium contacts, *Nano Lett.*, 2013, **13**, 100–105; (*b*) S. Kurtin and C. Mead, Surface barriers on layer semiconductors: GaS, GaSe, GaTe, *J. Phys. Chem. Solids*, 1969, **30**, 2007–2009; (*c*) A. Dimoulas, P. Tsipas, A. Sotiropoulos and E. Evangelou, Fermi-level pinning and charge neutrality level in germanium, *Appl. Phys. Lett.*, 2006, **89**, 252110.

66 C. Tang, Y. Min, C. Chen, W. Xu and L. Xu, Potential Applications of Heterostructures of TMDs with MXenes in Sodium-Ion and Na–$O_2$ Batteries, *Nano Lett.*, 2019, **19**, 5577–5586.

67 (*a*) D. Voiry, M. Salehi, R. Silva, T. Fujita, M. Chen, T. Asefa, V. B. Shenoy, G. Eda and M. Chhowalla, Conducting $MoS_2$ nanosheets as catalysts for hydrogen evolution reaction, *Nano Lett.*, 2013, **13**, 6222–6227; (*b*) J. Lee, P. Dak, Y. Lee, H. Park, W. Choi, M. A. Alam and S. Kim, Two-dimensional Layered $MoS_2$ Biosensors Enable Highly Sensitive Detection of Biomolecules, *Sci. Rep.*, 2014, **4**, 7352; (*c*) J. Martin, C. Donnet, T. Le Mogne and T. Epicier, Superlubricity of molybdenum disulphide, *Phys. Rev. B: Condens. Matter Mater. Phys.*, 1993, **48**, 10583; (*d*) T. Wang, S. Chen, H. Pang, H. Xue and Y. Yu, $MoS_2$-based nanocomposites for electrochemical energy storage, *Adv. Sci.*, 2017, **4**, 1600289; (*e*) L. Wang, L. Chen, S. L. Wong, X. Huang, W. Liao, C. Zhu, Y.-F. Lim, D. Li, X. Liu, D. Chi and K.-W. Ang, Electronic Devices and Circuits Based on Wafer-Scale Polycrystalline Monolayer $MoS_2$ by Chemical Vapor Deposition, *Adv. Electron. Mater.*, 2019, **5**, 1900393.

68 (*a*) Z. He and W. Que, Molybdenum disulfide nanomaterials: Structures, properties, synthesis and recent progress on hydrogen evolution reaction, *Appl. Mater. Today*, 2016, **3**, 23–56; (*b*) T. Stephenson, Z. Li, B. Olsen and D. Mitlin, Lithium ion battery applications of molybdenum disulfide ($MoS_2$) nanocomposites, *Energy Environ. Sci.*, 2014, **7**, 209–231.

69 J. M. Soon and K. P. Loh, Electrochemical double-layer capacitance of $MoS_2$ nanowall films, *Electrochem. Solid-State Lett.*, 2007, **10**, A250–A254.

70 G. Wang, J. Zhang, S. Yang, F. Wang, X. Zhuang, K. Müllen and X. Feng, Vertically Aligned $MoS_2$ Nanosheets Patterned on Electrochemically Exfoliated Graphene for High-Performance Lithium and Sodium Storage, *Adv. Energy Mater.*, 2018, **8**, 1702254.

71 (*a*) J.-Z. Wang, L. Lu, M. Lotya, J. N. Coleman, S.-L. Chou, H.-K. Liu, A. I. Minett and J. Chen, Development of $MoS_2$–CNT Composite Thin Film from Layered $MoS_2$ for Lithium Batteries, *Adv. Energy Mater.*, 2013, **3**, 798–805; (*b*) Z. Hu, X. Kuai, J. Chen, P. Sun, Q. Zhang, H.-H. Wu and L. Zhang, Strongly Coupled $MoS_2$ Nanocrystal/$Ti_3C_2$ Nanosheet Hybrids Enable High-Capacity Lithium-Ion Storage, *ChemSusChem*, 2020, **13**, 1485–1490; (*c*) Y. Chen, B. Song, X. Tang, L. Lu and J. Xue, Ultrasmall $Fe_3O_4$ nanoparticle/$MoS_2$ nanosheet composites with superior performances for lithium ion batteries, *Small*, 2014, **10**, 1536–1543; (*d*) L. David, R. Bhandavat and G. Singh, $MoS_2$/graphene composite paper for sodium-ion battery electrodes, *ACS Nano*, 2014, **8**, 1759–1770.

72 C. Shen, L. Wang, A. Zhou, H. Zhang, Z. Chen, Q. Hu and G. Qin, $MoS_2$-Decorated $Ti_3C_2$ MXene nanosheet as anode material in lithium-ion batteries, *J. Electrochem. Soc.*, 2017, **164**, A2654–A2659.

73 X. Wu, Z. Wang, M. Yu, L. Xiu and J. Qiu, Stabilizing the MXenes by carbon nanoplating for developing hierarchical nanohybrids with efficient lithium storage and hydrogen evolution capability, *Adv. Mater.*, 2017, **29**, 1607017.

74 N. H. Attanayake, S. C. Abeyweera, A. C. Thenuwara, B. Anasori, Y. Gogotsi, Y. Sun and D. R. Strongin, Vertically aligned $MoS_2$ on $Ti_3C_2$ (MXene) as an improved HER catalyst, *J. Mater. Chem. A*, 2018, **6**, 16882–16889.

75 K. Ma, H. Jiang, Y. Hu and C. Li, 2D Nanospace Confined Synthesis of Pseudocapacitance-Dominated $MoS_2$-in-$Ti_3C_2$ Superstructure for Ultrafast and Stable Li/Na-Ion Batteries, *Adv. Funct. Mater.*, 2018, **28**, 1804306.

76 (*a*) J. Bai, B. Zhao, S. Lin, K. Li, J. Zhou, J. Dai, X. Zhu and Y. Sun, Construction of hierarchical $V_4C_3$-MXene/$MoS_2$/C nanohybrids for high rate lithium-ion batteries, *Nanoscale*, 2020, **12**, 1144–1154; (*b*) J. Ren, H. Zong, Y. Sun, S. Gong, Y. Feng, Z. Wang, L. Hu, K. Yu and Z. Zhu, 2D organ-like molybdenum carbide (MXene) coupled with $MoS_2$ nanoflowers enhances the catalytic activity in the hydrogen evolution reaction, *CrystEngComm*, 2020, **22**, 1395–1403; (*c*) C. Chen, X. Xie, B. Anasori, A. Sarycheva, T. Makaryan, M. Zhao, P. Urbankowski, L. Miao, J. Jiang and Y. Gogotsi, $MoS_2$-on-MXene heterostructures as highly reversible anode materials for lithium-ion batteries, *Angew. Chem., Int. Ed.*, 2018, **57**, 1846–1850.

77 (*a*) J. Zhang, Q. Wang, L. Wang, X. A. Li and W. Huang, Layer-controllable $WS_2$-reduced graphene oxide hybrid nanosheets with high electrocatalytic activity for hydrogen evolution, *Nanoscale*, 2015, **7**, 10391–10397; (*b*) H. Liu, D. Su, G. Wang and S. Z. Qiao, An ordered mesoporous $WS_2$ anode material with superior electrochemical performance for lithium ion batteries, *J. Mater. Chem.*, 2012, **22**, 17437–17440; (*c*) C. Cong, J. Shang, Y. Wang and T. Yu, Optical Properties of 2D Semiconductor $WS_2$, *Adv. Opt. Mater.*, 2018, **6**, 1700767.

78 (*a*) L. Rapoport, Y. Bilik, Y. Feldman, M. Homyonfer, S. Cohen and R. Tenne, Hollow nanoparticles of $WS_2$ as potential solid-state lubricants, *Nature*, 1997, **387**, 791–793; (*b*) R. Bhandavat, L. David and G. Singh, Synthesis of surface-functionalized $WS_2$ nanosheets and performance as Li-ion battery anodes, *J. Phys. Chem. Lett.*, 2012, **3**, 1523–1530; (*c*) O. A. Abbas, I. Zeimpekis, H. Wang, A. H. Lewis, N. P. Sessions, M. Ebert, N. Aspiotis, C.-C. Huang, D. Hewak, S. Mailis and P. Sazio, Solution-Based Synthesis of Few-Layer $WS_2$ Large Area Continuous Films for Electronic Applications, *Sci. Rep.*, 2020, **10**, 1696; (*d*) N. Perea-López, A. L. Elías, A. Berkdemir, A. Castro-Beltran, H. R. Gutiérrez, S. Feng, R. Lv, T. Hayashi, F. López-Urías, S. Ghosh, B. Muchharla, S. Talapatra, H. Terrones and M. Terrones, Photosensor device based on few-layered $WS_2$ films, *Adv. Funct. Mater.*, 2013, **23**, 5511–5517; (*e*) J. Yang, L. Gao, C. Peng and W. Zhang, Construction of self-signal DNA electrochemical biosensor employing $WS_2$ nanosheets combined with $PIn_6COOH$, *RSC Adv.*, 2019, **9**, 9613–9619; (*f*) S. Ratha and C. S. Rout, Supercapacitor Electrodes Based on Layered Tungsten Disulfide-Reduced Graphene Oxide Hybrids Synthesized by a Facile Hydrothermal Method, *ACS Appl. Mater. Interfaces*, 2013, **5**, 11427–11433; (*g*) J. Lin, Z. Peng, G. Wang, D. Zakhidov, E. Larios, M. J. Yacaman and J. M. Tour, Enhanced Electrocatalysis for Hydrogen Evolution Reactions from $WS_2$ Nanoribbons, *Adv. Energy Mater.*, 2014, **4**, 1301875.

79 Y. Liu, N. Zhang, H. Kang, M. Shang, L. Jiao and J. Chen, $WS_2$ Nanowires as a high-performance anode for sodium–ion batteries, *Chem. – Eur. J.*, 2015, **21**, 11878–11884.

80 (*a*) Y. Liu, H. Wei, C. Wang, F. Wang, H. Wang, W. Zhang, X. Wang, C. Yan, B. H. Kim and F. Ren, Nitrogen-doped carbon coated $WS_2$ nanosheets as anode for high-performance sodium-ion batteries, *Front. Chem.*, 2018, **6**, 236; (*b*) Y. Huang, Y. Jiang, Z. Ma, Y. Zhang, X. Zheng, X. Yan, X. Deng, W. Xiao and H. Tang, Seaweed-liked $WS_2$/rGO enabling ultralong cycling life and enhanced rate capability for lithium-ion batteries, *Nanomaterials*, 2019, **9**, 469; (*c*) S. Bellani, F. Wang, G. Longoni, L. Najafi, R. Oropesa-Nunez, A. E. Del Rio Castillo, M. Prato, X. Zhuang, V. Pellegrini, X. Feng and F. Bonaccorso, $WS_2$–graphite dual-ion batteries, *Nano Lett.*, 2018, **18**, 7155–7164.

81 W. Su, S. Wang, L. Fu, F. Chen, K. Song, X. Huang and L. Yang, Growth of $WS_2$ flakes on $Ti_3C_2T_x$ Mxene Using Vapor Transportation Routine, *Coatings*, 2018, **8**, 281.

82 J.-J. Huang, X.-Q. Liu, F.-F. Meng, L.-Q. He, J.-X. Wang, J.-C. Wu, X.-H. Lu, Y.-X. Tong and P.-P. Fang, A facile method to produce $MoSe_2$/MXene hybrid nanoflowers with enhanced electrocatalytic activity for hydrogen evolution, *J. Electroanal. Chem.*, 2020, **856**, 113727.

 

83 N. Li, Y. Zhang, M. Jia, X. Lv, X. Li, R. Li, X. Ding, Y.-Z. Zheng and X. Tao, 1T/2H $MoSe_2$-on-MXene heterostructure as bifunctional electrocatalyst for efficient overall water splitting, *Electrochim. Acta*, 2019, **326**, 134976.

84 J. Xu, J. Shim, J. H. Park and S. Lee, MXene electrode for the integration of $WSe_2$ and $MoS_2$ field effect transistors, *Adv. Funct. Mater.*, 2016, **26**, 5328–5334.

85 P. G. Bruce, B. Scrosati and J. M. Tarascon, Nanomaterials for rechargeable lithium batteries, *Angew. Chem., Int. Ed.*, 2008, **47**, 2930–2946.

86 B. Scrosati and J. Garche, Lithium batteries: Status, prospects and future, *J. Power Sources*, 2010, **195**, 2419–2430.

87 (*a*) L. Shi and T. Zhao, Recent advances in inorganic 2D materials and their applications in lithium and sodium batteries, *J. Mater. Chem. A*, 2017, **5**, 3735–3758; (*b*) Y. Zhao, N. Yang, R. Yu, Y. Zhang, J. Zhang, Y. Li and D. Wang, Unique structural advances of graphdiyne for energy applications, *Energy Chem.*, 2020, **2**, 100041.

88 (*a*) R. Raccichini, A. Varzi, S. Passerini and B. Scrosati, The role of graphene for electrochemical energy storage, *Nat. Mater.*, 2015, **14**, 271–279; (*b*) P. Poizot, S. Laruelle, S. Grugeon, L. Dupont and J. Tarascon, Nano-sized transition-metal oxides as negative-electrode materials for lithium-ion batteries, *Nature*, 2000, **407**, 496–499.

89 J. Xiao, D. Choi, L. Cosimbescu, P. Koech, J. Liu and J. P. Lemmon, Exfoliated $MoS_2$ nanocomposite as an anode material for lithium ion batteries, *Chem. Mater.*, 2010, **22**, 4522–4524.

90 X. Xu, Z. Fan, S. Ding, D. Yu and Y. Du, Fabrication of $MoS_2$ nanosheet@ $TiO_2$ nanotube hybrid nanostructures for lithium storage, *Nanoscale*, 2014, **6**, 5245–5250.

91 (*a*) J. Li, Y. Hou, X. Gao, D. Guan, Y. Xie, J. Chen and C. Yuan, A three-dimensionally interconnected carbon nanotube/layered $MoS_2$ nanohybrid network for lithium ion battery anode with superior rate capacity and long-cycle-life, *Nano Energy*, 2015, **16**, 10–18; (*b*) J. Song, Y. Li, Z. Liu, C. Zhu, M. Imtiaz, X. Ling, D. Zhang, J. Mao, Z. Guo, S. Chu, P. Liu and S. Zhu, Enhanced lithium storage for $MoS_2$-based composites *via* a vacancy-assisted method, *Appl. Surf. Sci.*, 2020, **515**, 146103.

92 J. Luo, X. Tao, J. Zhang, Y. Xia, H. Huang, L. Zhang, Y. Gan, C. Liang and W. Zhang, $Sn^{4+}$ ion decorated highly conductive $Ti_3C_2$ MXene: promising lithium-ion anodes with enhanced volumetric capacity and cyclic performance, *ACS Nano*, 2016, **10**, 2491–2499.

93 G. Du, M. Tao, W. Gao, Y. Zhang, R. Zhan, S. Bao and M. Xu, Preparation of $MoS_2/Ti_3C_2T_x$ composite as anode material with enhanced sodium/lithium storage performance, *Inorg. Chen. Front.*, 2019, **6**, 117–125.

94 Y. Wu and Y. Yu, 2D material as anode for sodium ion batteries: Recent progress and perspectives, *Energy Storage Mater.*, 2019, **16**, 323–343.

95 N. K. Chaudhari, H. Jin, B. Kim, D. San Baek, S. H. Joo and K. Lee, MXene: an emerging two-dimensional material for future energy conversion and storage applications, *J. Mater. Chem. A*, 2017, **5**, 24564–24579.

96 (*a*) M. Xu, N. Bai, H.-X. Li, C. Hu, J. Qi and X.-B. Yan, Synthesis of MXene-supported layered $MoS_2$ with enhanced electrochemical performance for Mg batteries, *Chin. Chem. Lett.*, 2018, **29**, 1313–1316; (*b*) Y. Zhang, Z. Mu, C. Yang, Z. Xu, S. Zhang, X. Zhang, Y. Li, J. Lai, Z. Sun, Y. Yang, Y. Chao, C. Li, X. Ge, W. Yang and S. Guo, Rational Design of MXene/1T-2H $MoS_2$–C Nanohybrids for High-Performance Lithium–Sulfur Batteries, *Adv. Funct. Mater.*, 2018, **28**, 1707578.

97 (*a*) J.-w. Seo, J.-t. Jang, S.-w. Park, C. Kim, B. Park and J. Cheon, Two-Dimensional $SnS_2$ Nanoplates with Extraordinary High Discharge Capacity for Lithium Ion Batteries, *Adv. Mater.*, 2008, **20**, 4269–4273; (*b*) W. Sun, X. Rui, D. Yang, Z. Sun, B. Li, W. Zhang, Y. Zong, S. Madhavi, S. Dou and Q. Yan, Two-Dimensional Tin Disulfide Nanosheets for Enhanced Sodium Storage, *ACS Nano*, 2015, **9**, 11371–11381.

98 J. R. Miller and P. Simon, Electrochemical capacitors for energy management, *Science*, 2008, **321**, 651–652.

99 (*a*) S. Bose, T. Kuila, A. K. Mishra, R. Rajasekar, N. H. Kim and J. H. Lee, Carbon-based nanostructured materials and their composites as supercapacitor electrodes, *J. Mater. Chem.*, 2012, **22**, 767–784; (*b*) Y. Tao, X. Xie, W. Lv, D.-M. Tang, D. Kong, Z. Huang, H. Nishihara, T. Ishii, B. Li, D. Golberg, F. Kang, T. Kyotani and Q.-H. Yang, Towards ultrahigh volumetric capacitance: graphene derived highly dense but porous carbons for supercapacitors, *Sci. Rep.*, 2013, **3**, 2975.

100 V. Subramanian, S. C. Hall, P. H. Smith and B. Rambabu, Mesoporous anhydrous $RuO_2$ as a supercapacitor electrode material, *Solid State Ionics*, 2004, **175**, 511–515.

101 (*a*) A. Ostadhossein, J. Guo, F. Simeski and M. Ihme, Functionalization of 2D materials for enhancing OER/ORR catalytic activity in Li–oxygen batteries, *Commun. Chem.*, 2019, **2**, 95; (*b*) Z. W. Seh, K. D. Fredrickson, B. Anasori, J. Kibsgaard, A. L. Strickler, M. R. Lukatskaya, Y. Gogotsi, T. F. Jaramillo and A. Vojvodic, Two-Dimensional Molybdenum Carbide (MXene) as an Efficient Electrocatalyst for Hydrogen Evolution, *ACS Energy Lett.*, 2016, **1**, 589–594; (*c*) D. R. Cummins, U. Martinez, A. Sherehiy, R. Kappera, A. Martinez-Garcia, R. K. Schulze, J. Jasinski, J. Zhang, R. K. Gupta, J. Lou, M. Chhowalla, G. Sumanasekera, A. D. Mohite, M. K. Sunkara and G. Gupta, Efficient hydrogen evolution in transition metal dichalcogenides via a simple one-step hydrazine reaction, *Nat. Commun.*, 2016, **7**, 11857; (*d*) F. Wang, T. A. Shifa, X. Zhan, Y. Huang, K. Liu, Z. Cheng, C. Jiang and J. He, Recent advances in transition-metal dichalcogenide based nanomaterials for water splitting, *Nanoscale*, 2015, **7**, 19764–19788; (*e*) X. Xu, B. Sun, Z. Liang, H. Cui and J. Tian, High-Performance Electrocatalytic Conversion of $N_2$ to $NH_3$ Using 1T-MoS2 Anchored on $Ti_3C_2$ MXene under Ambient Conditions, *ACS Appl. Mater. Interfaces*, 2020, **12**, 26060–26067.

102 R. B. Rakhi, B. Ahmed, M. N. Hedhili, D. H. Anjum and H. N. Alshareef, Effect of Postetch Annealing Gas Composition on the Structural and Electrochemical Properties of

$Ti_2CT_x$ MXene Electrodes for Supercapacitor Applications, *Chem. Mater.*, 2015, **27**, 5314–5323.

103 Y. Lee, S. J. Kim, Y.-J. Kim, Y. Lim, Y. Chae, B.-J. Lee, Y.-T. Kim, H. Han, Y. Gogotsi and C. W. Ahn, Oxidation-resistant titanium carbide MXene films, *J. Mater. Chem. A*, 2020, **8**, 573–581.

104 K. R. G. Lim, A. D. Handoko, L. R. Johnson, X. Meng, M. Lin, G. S. Subramanian, B. Anasori, Y. Gogotsi, A. Vojvodic and Z. W. Seh, 2H-$MoS_2$ on $Mo_2CT_x$ MXene Nanohybrid for Efficient and Durable Electrocatalytic Hydrogen Evolution, *ACS Nano*, 2020, **14**, 16140–16155.

105 (*a*) L. Huang, L. Ai, M. Wang, J. Jiang and S. Wang, Hierarchical $MoS_2$ nanosheets integrated $Ti_3C_2$ MXenes for electrocatalytic hydrogen evolution, *Int. J. Hydrogen Energy*, 2019, **44**, 965–976; (*b*) J. Liang, C. Ding, J. Liu, T. Chen, W. Peng, Y. Li, F. Zhang and X. Fan, Heterostructure engineering of Co-doped $MoS_2$ coupled with $Mo_2CT_x$ MXene for enhanced hydrogen evolution in alkaline media, *Nanoscale*, 2019, **11**, 10992–11000.

106 J. Zhang, T. Wang, P. Liu, S. Liu, R. Dong, X. Zhuang, M. Chen and X. Feng, Engineering water dissociation sites in $MoS_2$ nanosheets for accelerated electrocatalytic hydrogen production, *Energy Environ. Sci.*, 2016, **9**, 2789–2793.

107 (*a*) X. Yang, Q. Jia, F. Duan, B. Hu, M. Wang, L. He, Y. Song and Z. Zhang, Multiwall carbon nanotubes loaded with $MoS_2$ quantum dots and MXene quantum dots: Non–Pt bifunctional catalyst for the methanol oxidation and oxygen reduction reactions in alkaline solution, *Appl. Surf. Sci.*, 2019, **464**, 78–87; (*b*) X. Pang, T. Wu, Y. Gu, D. Wang, X. Che, D. Sun and F. Huang, $Nb_2Se_2C$: a new compound as a combination of transition metal dichalcogenide and MXene for oxygen evolution reaction, *Chem. Commun.*, 2020, **56**, 9036–9039.

108 (*a*) W. Y. Chen, X. Jiang, S.-N. Lai, D. Peroulis and L. Stanciu, Nanohybrids of a MXene and transition metal dichalcogenide for selective detection of volatile organic compounds, *Nat. Commun.*, 2020, **11**, 1302; (*b*) F. Alimohammadi, M. S. Gh, N. H. Attanayake, A. C. Thenuwara, Y. Gogotsi, B. Anasori and D. R. Strongin, Antimicrobial Properties of 2D $MnO_2$ and $MoS_2$ Nanomaterials Vertically Aligned on Graphene Materials and $Ti_3C_2$ MXene, *Langmuir*, 2018, **34**, 7192–7200; (*c*) P. Zhao, H. Jin, X. Lv, B. Huang, Y. Ma and Y. Dai, Modified MXene: promising electrode materials for constructing Ohmic contacts with $MoS_2$ for electronic device applications, *Phys. Chem. Chem. Phys.*, 2018, **20**, 16551–16557; (*d*) A. Shahzad, J. Jang, S.-R. Lim and D. S. Lee, Unique selectivity and rapid uptake of molybdenum-disulfide-functionalized MXene nanocomposite for mercury adsorption, *Environ. Res.*, 2020, **182**, 109005.

109 (*a*) A. D. Handoko, K. D. Fredrickson, B. Anasori, K. W. Convey, L. R. Johnson, Y. Gogotsi, A. Vojvodic and Z. W. Seh, Tuning the Basal Plane Functionalization of Two-Dimensional Metal Carbides (MXenes) To Control Hydrogen Evolution Activity, *ACS Appl. Energy Mater.*, 2018, **1**, 173–180; (*b*) P. Li, J. Zhu, A. D. Handoko, R. Zhang, H. Wang, D. Legut, X. Wen, Z. Fu, Z. W. Seh and Q. Zhang, High-throughput theoretical optimization of the hydrogen evolution reaction on MXenes by transition metal modification, *J. Mater. Chem. A*, 2018, **6**, 4271–4278.

110 X. Liang, A. Garsuch and L. F. Nazar, Sulfur Cathodes Based on Conductive MXene Nanosheets for High-Performance Lithium–Sulfur Batteries, *Angew. Chem., Int. Ed.*, 2015, **54**, 3907–3911.

111 J. Chen, K. Chen, D. Tong, Y. Huang, J. Zhang, J. Xue, Q. Huang and T. Chen, CO2 and temperature dual responsive "Smart" MXene phases, *Chem. Commun.*, 2015, **51**, 314–317.

112 N. Abidi, K. R. G. Lim, Z. W. Seh and S. N. Steinmann, Atomistic modeling of electrocatalysis: Are we there yet?, *WIREs Comput. Mol. Sci.*, 2020, e1499, DOI: 10.1002/wcms.1499.

113 Y.-Z. Zhang, Y. Wang, Q. Jiang, J. K. El-Demellawi, H. Kim and H. N. Alshareef, MXene Printing and Patterned Coating for Device Applications, *Adv. Mater.*, 2020, **32**, 1908486.

 